

General Disclaimer

One or more of the Following Statements may affect this Document

- This document has been reproduced from the best copy furnished by the organizational source. It is being released in the interest of making available as much information as possible.
- This document may contain data, which exceeds the sheet parameters. It was furnished in this condition by the organizational source and is the best copy available.
- This document may contain tone-on-tone or color graphs, charts and/or pictures, which have been reproduced in black and white.
- This document is paginated as submitted by the original source.
- Portions of this document are not fully legible due to the historical nature of some of the material. However, it is the best reproduction available from the original submission.

--	--	--	--	--	--

(NASA-CR-132623) AN INVESTIGATION OF ESSA 7
RADIATION DATA FOR USE IN LONG-TERM EARTH
ENERGY EXPERIMENTS, PHASES 1 AND 2 Final
Report (Drexel Univ.) 72 p HC \$4.25

N75-28998

Unclas

CSCI 03B G3/93 31370

AN INVESTIGATION OF ESSA VII RADIATION
DATA FOR USE IN LONG-TERM EARTH
ENERGY EXPERIMENTS

By Frederick B. House

Final Report
Phases I and II

Prepared under Contract No. NAS1-11871 by
Department of Physics and Atmospheric Science
Drexel University
Philadelphia, Pennsylvania 19104

for

NATIONAL AERONAUTICS AND SPACE ADMINISTRATION

FOREWORD

The present report contains the results of an investigation of ESSA VII Satellite radiation data for use in long-term earth energy experiments, performed under Langley Research Contract No. NAS1-11871 for the National Aeronautics and Space Administration.

This research study, performed by Drexel University, is one part of a much larger effort by several institutions, including Colorado State University, Virginia Polytechnic Institute and State University, Link Temco Vought as well as cognizant personnel at NASA Langley Research Center. This team is studying satellite systems for performing long-term earth radiation balance measurements over geographical areas, hemispheres, and the entire earth for periods of 10 to 30 years. A major portion of the total effort is responsive to the AAFE proposal and the proposed LZEEBE system (House and Sweet, 1973).

This investigation was conducted to provide necessary design data for use in developing the LZEEBE system. ESSA VII satellite employed plate and cone radiometers to measure earth albedo and emitted radiation. Each instrument had a black and white radiometer which discriminated the components of albedo and emitted radiation, and is identical in most respects to the proposed black and white balloons of the LZEEBE system. Earth measurements were made continuously from ESSA VII for ten months.

The express purpose of this investigation is to obtain the ESSA VII raw data and process it to a point where it can be further analyzed for:

- development of long-term earth energy experiments
- document climate trends

In addition to satisfying the immediate requirements of the contractual statement of work, the research effort has included other areas of

FOREWORD (Continued)

investigation. This report is one of three companion reports which together constitute the final report of phases I and II of subject contract. The two other reports are entitled; "Steady-State Solution to the Conduction Problem of a Spherical Balloon Radiometer," published as NASA CR-132624, and "Our Contaminated Atmosphere - The Danger of Climate Change," published as NASA CR-132625.

Gratitude is extended to several NASA/LARC personnel for their encouragement, interest, stimulating discussions and suggestions provided during the present investigation. Among these scientific personnel are included: Messrs. George Sweet (technical monitor), Charles Woerner and Jack Cooper.

TABLE OF CONTENTS

	<u>Page</u>
FOREWORD	i
TABLE OF CONTENTS	iii
LIST OF FIGURES	iv
LIST OF TABLES	v
LIST OF SYMBOLS	vi
INTRODUCTION	1
ESSA VII INSTRUMENTATION	6
RADIOMETER CONSTRUCTION AND VIEWING CHARACTERISTICS	7
ABSORBED IRRADIANCE ON A UNIT DETECTOR AREA	9
PROCESSING ESSA VII RAW DATA	12
PREFLIGHT INSTRUMENT CALIBRATION	19
LONGWAVE COLOR CONSTANTS	19
POWER EXCHANGE BETWEEN RADIOMETER AND CASE	21
INFLIGHT CALIBRATION PROCEDURES	28
CALIBRATION OF MASS CONSTANTS	29
CALIBRATION OF SHORTWAVE COLOR CONSTANTS	35
ANALYSIS OF ERRORS	37
CORRELATION OF PLATE AND CONE MEASUREMENTS	40
STUDY CONCLUSIONS RELATED TO LZEEBE SYSTEM CONSIDERATIONS	43
ENGINEERING DESIGN CONSIDERATIONS - LZEEBE SYSTEM	45
FLIGHT OPERATIONS - LZEEBE SYSTEM	46
REFERENCES	47
APPENDIX A - COMPUTER SOFTWARE FOR PRELIMINARY PROCESSING OF ESSA VII SATELLITE DATA	48

LIST OF FIGURES

<u>Figure</u>		<u>Page</u>
1.	Radiant power balance on an earth surface element	2
2.	Conceptual drawing of ESSA VII satellite showing cartwheel configuration, orbital plane and earth viewed area	8
3.	Expanded view of ESSA VII plate radiometer components (a), and the radiometer with cone optics (b). Taken from Nelson and Parent (1967)	10
4.	Spectral absorptance properties of the black and white ESSA radiometers	22
5.	Variation in absorptivity and emissivity with temperature - black radiometers	23
6.	Variation in absorptivity and emissivity with temperature - white radiometers	24
7.	Simulated ingress data for a LZEEBE balloon radiometer	32
8.	Variation in mass term with temperature for the white and black radiometers	34
9.	Concept of shortwave color constant calibration procedure	36
10.	Correlation of white plate vs. black plate radiometers	41
11.	Correlation of black plate vs. black cone radiometers	44

LIST OF TABLES

<u>Table</u>		<u>Page</u>
1.	Available ESSA VII satellite data	15
2.	Inconsistent or missing ESSA VII satellite data	16
3.	Longwave color constants for ESSA VII radiometers	25
4.	Case radiation constants for ESSA VII radiometers	27

LIST OF SYMBOLS

Symbol	Definition	First used in	
		Equation	on Page
Q_n	Net radiant power density, watts/m ²	(1)	1
H_0	Direct solar irradiance normal to an area, watts/m ²	Figure 1	2
H_s	Direct solar irradiance, $H_s = H_0 \cos \phi$	(1)	1
ϕ	Angle to normal of surface area, deg.	Figure 1	2
W_r	Radiant power density of reflected solar (shortwave) radiation	(1)	1
W_e	Radiant power density of emitted longwave radiation	(1)	1
A	Earth albedo, $A = W_r/H_s$	(1)	1
$\bar{\alpha}_e$	Average broad-band absorptivity to longwave radiation	(2)	11
F_e	Shape factor from satellite radiometer to earth (longwave)	(2)	11
$\bar{\alpha}_s$	Average broad-band absorptivity to direct solar irradiance	(2)	11
F_s	Shape factor from satellite radiometer to sun	(2)	11
$\bar{\alpha}_r$	Average broad-band absorptivity to shortwave radiation	(2)	11
F_r	Shape factor from satellite radiometer to earth (shortwave)	(2)	11
W_d	Radiant power loss per unit detector area	(2)	11
ϵ	Emissivity of detector	(3)	12
σ	Stefan-Boltzmann Constant, $\sigma = 5.6697 \times 10^{-8}$ watts/m ² - K ⁴	(3)	12
T	Temperature of the radiometer, K	(3)	12
M(T)	Mass term, Joules/m ² -K	(3)	12
\dot{T}	Temperature change with time, $\dot{T} \equiv \frac{dT}{dt}$, K/sec	(3)	12
t	Time, sec	Text	--
R	Case radiation constant	(3)	12

LIST OF SYMBOLS (Continued)

<u>Symbol</u>	<u>Definition</u>	<u>Equation</u>	<u>Page</u>
T_c	Case temperature, K	(3)	12
λ	Wavelength, microns	(4)	20
$\alpha(\lambda)$	Spectral absorptivity of radiometer	(4)	20
$N(\lambda)$	Spectral radiance from homogeneous earth field, watts/m ² - Ster	(4)	20
$\epsilon(\lambda)$	Spectral emissivity of radiometer	(5)	20
$B(\lambda, T)$	Planck's black body function, watts/m ² - Ster	(5)	20
ϵ_d	Emissivity of radiometer (daytime mode)	Table 3	25
ϵ_n	Emissivity of radiometer (nighttime mode)	Table 3	25
T_s	Source temperature of chamber, K	(7)	26
\dot{W}_e	Longwave radiation gradient during thermal transition, $\dot{W}_e = \frac{dW_e}{dt}$, watts/m ² - sec	Text	30

INTRODUCTION

Radiation balance measurements from satellites are worthwhile scientific experiments to perform. The radiation balance, defined as the difference between absorbed solar radiation and emitted thermal radiation at the outer boundary of the earth-atmosphere system, is the source of power that drives the atmospheric heat engine. Temporal and geographical distributions of this net heating and cooling produce a broad spectrum of weather events. For example, long-term changes in the global radiation balance result in climatic variations. Heating in equatorial regions and cooling in polar regions cause thermal contrasts at the surface and in the atmosphere which produce seasonal changes. The radiation balance is one diabatic component of atmospheric motion which influences general circulation patterns over time scales of several weeks. Geographical distributions of the radiation balance may affect the development of smaller scale features such as synoptic and mesoscale weather events. Observations of the global distribution of this differential heating and cooling at the outer boundary of the atmosphere represent valuable scientific information.

The net rate of radiant power gain for an area element of the earth on a specified time scale is determined by the relation:

$$Q_n = H_s - (W_r + W_e) = (1-A) H_s - W_e \quad (1)$$

where the parameters are shown schematically in Figure 1. All symbols in equation (1) and others to follow are defined in the List of Symbols in the front matter of this report.

When integrated over the earth, Q_n describes the radiant energy exchange between the planet earth and space. This quantity is determined

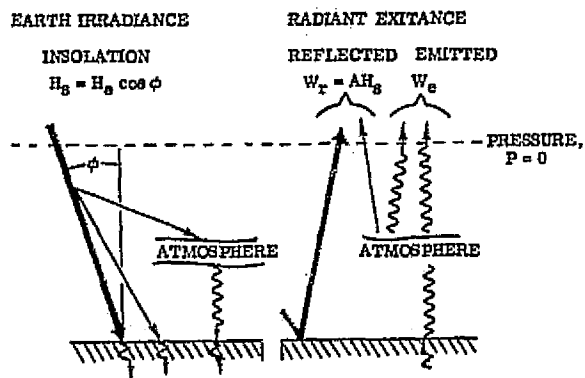


Figure 1. Radiant power balance on an earth surface element.

by the fluxes of incoming solar electromagnetic radiation, H_s , reflected solar radiation W_r , and emitted long-wave radiation, W_e , crossing a horizontal element of area just outside the earth's atmosphere ($P = 0$). Representative values of these fluxes are: 1353 w/m^2 for H_s , 240 w/m^2 for W_e , and about 400 w/m^2 for W_r at a location where $\phi = 0$. Other possible radiant power sources such as the fluxes of particle radiation and of electromagnetic radiation from the moon and all other stars, and the heat flux from the earth's interior are comparatively small.

Satellite experiments are designed to measure the following:

- The infrared radiant exitance, W_e , and
- The planetary albedo, A ; where $A = W_r/H_s$.

Satellites offer an ideal platform from which to perform radiation balance measurements owing to their locations outside the outer boundary of the atmosphere. In addition, polar orbiting satellites provide measurement coverage of the entire earth, but at nearly the same local time during the day or night.

Notwithstanding the above attractive possibilities of performing radiation balance measurements from satellites, certain desirable applications of the data are somewhat elusive. Problems such as the frequency and geographical distribution of sampling, spatial resolution of the measurements, and experimental accuracy pertain to both the design of experiments and the scientific applications of the data. As Möller and Raschke (1969) have pointed out, high accuracies of the components in equation (1) may be required. For example, if the global mean net radiation is 0.7 watt/m^2 and an accuracy of 20 percent is desired, the global means of W_e and $(H_s - W_r)$ are required to within an accuracy of 0.3 percent.

Obtaining these accuracies and properly sampling the earth both temporally and with sufficient spatial resolution are exceedingly difficult, even with highly sophisticated instrumentation and a multiple satellite system.

The foregoing discussions involving the applicability and associated problems of observations from satellites has been presented so that the radiation balance measurements from ESSA weather satellites can be viewed in proper perspective. Instrumentation on these satellites provide observations of W_r , W_e and an estimate of the difference ($H_s - W_r$). The radiometers have broad-band spectral and low-resolution spatial characteristics. The parametric measurements of radiant power density at satellite altitude involve an integrated average of irradiances from the earth-viewed area, as influenced by the optical characteristics of the radiometers and the rotation of the satellite. These measurements can be scaled to any arbitrary reference spheroid to account for variations in satellite altitude. They are useful in the study of the global radiation balance and can probably be employed effectively in studies related to general circulation patterns.

The major objective of the current research effort is to obtain ESSA VII raw data and process it to a point where it can be further analyzed for the development of long-term earth energy experiments and documentation of climate trends. Specific tasks in this regard are outlined in the following statement-of-work:

1. Obtain ESSA VII tapes from NESS/NOAA.
2. Develop computer software to preprocess the data tapes.
3. Determine inflight calibration constants, correlate them with

- preflight calibrations and apply the results to the raw data.
4. Perform color corrections to the white detectors.
 5. Correlate plate and cone measurements.
 6. Perform an error analysis.
 7. Develop a statistical technique for performing co-spectrum and cross-spectrum analyses.
 8. Insure that magnetic tapes can be processed with LRC computers.
 9. Evaluate the accuracy of inflight methods for calibrating radiometers and color constants.
 10. Provide guidelines for system design and flight operations of a proposed satellite system for measuring the long-term earth energy budget.

It should be emphasized that the procedures discussed in the following sections of the report find direct application to the balloon radiometers of the LZEEBE system. In fact, the geometrical viewing considerations of a spinning flat plate on ESSA VII are more complicated than the omni-directional spherical geometry of LZEEBE.

A description of ESSA VII radiometers is presented first before discussing processing aspects of ESSA VII data. This is followed by a description of preflight instrument calibration and then a new method for inflight calibration of shortwave color constants, developed expressly with the LZEEBE system in mind, using ESSA VII data. Comments concerning the correlation of cone and plate measurements follow the above sections. Preliminary conclusions concerning system design and flight operations of measurement systems conclude the main text of the report.

ESSA VII INSTRUMENTATION

Historically, the measurement concept employed on LZEEBE and ESSA VII satellites is similar to earlier instrument packages flown on Explorer VII satellite and TIROS III, IV and VII satellites (Suomi, 1958; Suomi, 1961). Two radiometers having different optical surface properties are used to discriminate the upwelling earth flux into its shortwave, W_r and longwave, W_e components. Exposure of both radiometers to direct solar irradiance provides additional information concerning the magnitude of $(H_s - W_r)$ in equation (1). Employing various combinations of these measurements, it is also possible to determine the earth's albedo and the radiation balance parameter, providing assumptions concerning the angular variation of earth radiant exitance are made.

Measurement theory for calculating the above parameters from telemetry data has been discussed by several authors (Suomi, 1961; Weinstein and Suomi, 1961; Bignell, 1962; House, 1965; MacDonald, 1966; Suomi, et al., 1967; Vonder Haar, 1968; House, 1968; House, 1970). These mathematical techniques apply to either mirror-backed hemispherical radiometers, flux plate radiometers (both mounted on a rotating satellite frame of reference) and isolated, omni-directional spheres of the LZEEBE system.

The following discussion of this section includes the radiometer construction and viewing characteristics of ESSA VII instrumentation, and the general equation of absorbed irradiance on a unit detector area.

RADIOMETER CONSTRUCTION AND VIEWING CHARACTERISTICS

A detailed description of the instrument package on ESSA weather satellites has been presented in detail by Nelson and Parent (1967). Briefly, the experimental configuration involves a set of four radiometers on each of two opposite sides of the satellite where each detector is connected electrically in series with its mate on the other side. The detector arrays are mounted on the circumference of the cartwheel satellite, perpendicular to the spin axis which is normal to the orbital plane (see Figure 2). The temperatures of the detectors and housings supporting the detectors are the measured signals at the spacecraft.

Each detector alternately views the earth and space during a rotation. Since the rotational period is relatively slow, about once every 6.5 seconds, a single detector would have a modulating signal of about 1°C to 3°C in phase with the rotational period. Since the integrating time of a temperature observation is relatively short compared to the rotational period, the thermal variation magnitude is significant in terms of earth flux calculations. However, the design of the experiment is such that the matched detector on the opposite side compensates for the modulating signal. As a result, the measured signal (temperature) is treated as being independent of the spacecraft's rotation and is interpreted as an average temperature over the time span of the rotational period.

Each of the two opposing arrays contain four flux plate detectors which are thermally isolated from the spacecraft as effectively as possible. Two of the four detectors in an array are exposed to a hemisphere

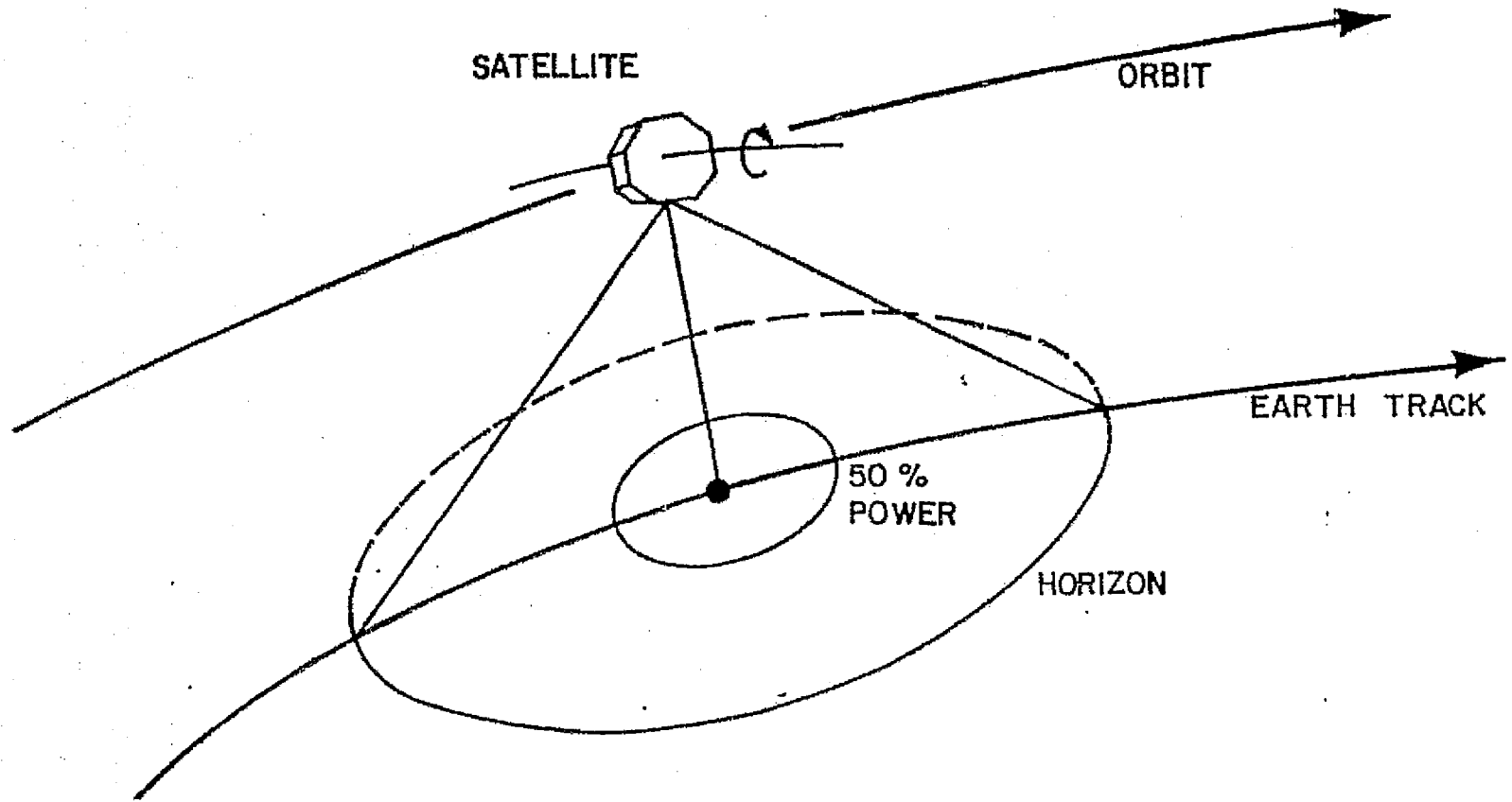


Figure 2. Conceptual drawing of ESSA VII satellite showing cart-wheel configuration, orbital plane and earth-viewed area.

field-of-view (Figure 3a) whereas the other two detectors are located at the apex of highly reflecting cones (Figure 3b). For convenience, these radiometers are referred to as "plate" and "cone" radiometers, respectively.

Each detector pair has different optical surface properties in order to discriminate the radiation balance components. One surface is painted black which has the property of being equally sensitive to both shortwave and longwave radiation. The other detector of the pair is an anodized aluminum or "white" surface which has the property of reflecting short-wave radiation and absorbing longwave radiation. Both of the cone and plate radiometers have black and white optical surfaces.

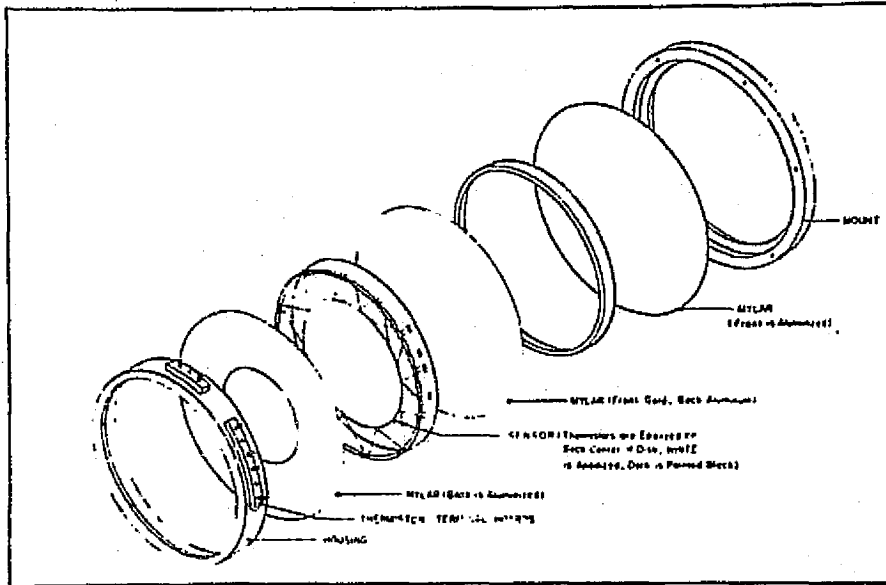
ABSORBED IRRADIANCE ON A UNIT DETECTOR AREA

During the course of a satellite orbit, between one and three sources of irradiance may be absorbed by the radiometers. If the satellite is in the earth's shadow (nighttime mode) only one source is present, W_e . Just before ingress into, and egress from, the earth's umbra (calibration mode), two sources are present, W_e and H_s . During the remainder of the orbit (day-time mode) all sources are present, W_e , H_s and W_r .

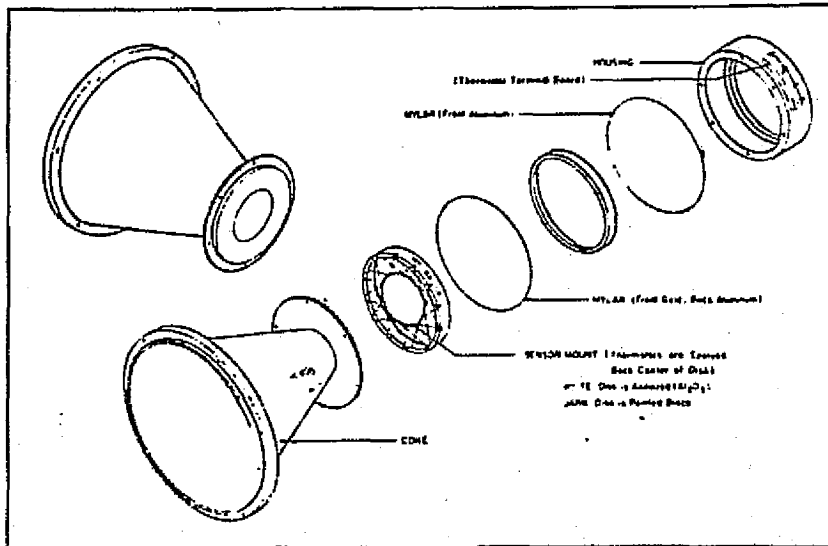
Since the instrumentation employed on ESSA VII comprise radiative equilibrium bolometers, all absorbed irradiances during the satellite orbit are balanced by an equal radiant power loss per unit detector area W_d . The general mathematical expression for this balance is

$$\bar{\alpha}_e F_e W_e + \bar{\alpha}_s F_s H_s + \bar{\alpha}_r F_r W_r = W_d \quad (2)$$

The three terms to the left of equation (2) comprise longwave emitted, direct solar and reflected shortwave irradiances, respectively.



(a)



(b)

Figure 3. Expanded view of ESSA VII plate radiometer components (a) and the radiometer with cone optics (b). Taken from Nelson and Parent (1967).

For the plate radiometers on ESSA VII, the first term applies during nighttime mode, the first two terms apply during calibration mode near satellite ingress and egress, and all three terms apply during daytime mode observations. On the other hand, the optics of the cone radiometers shield the detectors from direct solar irradiance. Thus, only the first and third terms of equation (2) apply during the daytime mode.

It should be clearly emphasized that some rather drastic assumptions are being made when equation (2) is applied to real radiation balance measurements. It is assumed that the optical properties of the detector over both the broad shortwave and longwave regions of the spectrum can be approximated by average absorptivities $\bar{\alpha}_s$ or $\bar{\alpha}_r$ and $\bar{\alpha}_e$, respectively. For this to hold, the optical surfaces must have uniform spectral response over both broad-band regions since spectral irradiances in both regions vary as a function of wavelength. If this is not the case, some error will be introduced into the calculated radiant power densities W_e and W_r .

A second major assumption is incorporated in the use of the shape factor F . The shape factor is a geometric term coupling all the angular absorbing properties of the detector configuration as well as assuming knowledge of any angular characteristics of the earth radiation field impinging on the detector. Certainly, the shape factor will vary both in time and geographical location, especially F_r which incorporates the anisotropic reflecting properties of the earth and atmosphere. The validity of both assumptions concerning constant absorptivities and shape factors should be investigated in depth in future research efforts

Returning again to equation (2), the radiant power loss by a unit detector area W_d is expressed as

$$\frac{W_d}{\epsilon} = \sigma T^4 + M(T)\dot{T} + R(\sigma T^4 - \sigma T_c^4) \quad (3)$$

T is the measured temperature of the radiometer and T_c is the case temperature supporting the radiometer. These two temperatures are telemetered to earth. The mass constant $M(T)$ and the case radiation constant R are subjects of inflight and preflight calibration procedures, respectively, to be discussed in sections to follow.

PROCESSING ESSA VII RAW DATA

One of the major accomplishments during this investigation was the successful processing of 20 reels of ESSA VII raw data. It required about nine months of effort to overcome many unexpected peculiarities in the data format. Certainly the documented format was far different than that which was really on the reels of tape, especially the positioning of end-of-file indicators. Many times these would occur in the middle of a satellite readout or there would be two or three end-of-file indicators at the end of each readout. One cannot appreciate the exasperation of processing data until he has attempted it himself.

Part of the data processing effort included the development of tables which convert raw counts from the satellite to appropriate calibrated temperatures. In order to accomplish this task, hundreds of calibration points were plotted for each radiometer and case. Smooth curves were drawn through the average trend of these points. In some cases, there were obvious errors in the calibration data. All such points which were

completely inconsistent with the other data were discarded.

Details of the software used in processing the ESSA VII data are presented in Appendix A. The processed data are stored on 20 computer tapes in FORTRAN readable format which can be utilized on any computing system. Copies of these data are available from Drexel University upon request.

During the data processing, each satellite readout is analyzed for bad data and consistency with orbit ephemeris. The status of each readout was listed, independent of writing information on the new tapes, so that a formal documentation of data quality is available for future processing. For example, if a readout was found to be inconsistent with the ephemeris, the processing of that readout was terminated and an appropriate note of termination was printed on the data quality documentation listing. Then processing of the next readout was started.

A tabulation of ESSA VII data available for future processing is presented in Table 1. Useful data are available during the period 3 Sept. 1968 - 22 June 1969. Evidently there was a problem with the tape recorder during the latter stages of data acquisition. There were several mismatches of observations and ephemeris information, starting on tape #1018. Tape #1019 has only 4 days of data. There is an eleven day gap in data between the end of #1019 and the start of tape #1020 which contains the last eight days of data.

The detailed information presented in Table II tabulates specific readouts that were judged not suitable for future processing and also accounts for gaps in the data. Each tape covers about a period of one half month. There were several bad readouts on the first tape #1001 and on tapes #1015 - #1020. The record shows that data recovery diminished

during the last 2 1/2 months of operation. However, the amount of useable data for future investigations is quite good when one considers all the number of useable readouts. During the entire period of data, there is 88% useable data. Of the remaining 12%, about 2% comprise inconsistent orbits and 10% of the readouts are missing. If one considers the time period between 3 September 1968 and 31 May 1969, the useable data comprises 93% of the period. It must be remembered that a small portion of each readout is lost during each interrogation from the ground control.

TABLE 1

Available ESSA VII Satellite Data

Tape ID	Calendar Dates	Julian Days		Orbit Numbers	
		Begin	End	Begin	End
1001	3 Sept. - 17 Sept. '68	18	32	231	400
1002	17 Sept. - 30 Sept. '68	32	45	400	570
1003	30 Sept. - 15 Oct. '68	45	60	570	758
1004	15 Oct. - 31 Oct. '68	60	76	750	954
1005	31 Oct. - 15 Nov. '68	76	91	954	1146
1006	15 Nov. - 30 Nov. '68	91	106	1146	1334
1007	30 Nov. - 15 Dec. '68	106	121	1334	1521
1008	15 Dec. - 31 Dec. '68	121	137	1521	1722
1009	31 Dec. - 15 Jan. '69	137	152	1722	1910
1010	15 Jan. - 31 Jan. '69	152	168	1910	2110
1011	31 Jan. - 15 Feb. '69	168	183	2110	2298
1012	15 Feb. - 28 Feb. '69	183	196	2298	2458
1013	1 Mar. - 15 Mar. '69	197	211	2462	2645
1014	15 Mar. - 31 Mar. '69	211	227	2645	2849
1015	31 Mar. - 14 Apr. '69	227	241	2849	3029
1016	15 Apr. - 30 Apr. '69	242	257	3035	3222
1017	30 Apr. - 15 May '69	257	272	3222	3409
1018	15 May - 31 May '69	272	288	3409	3611
1019	31 May - 4 June '69	288	292	3611	3655
1020	15 June - 22 June '69	303	310	3797	3888

TABLE 2

Inconsistent or Missing ESSA VII Satellite Data

Tape ID	Julian Day	Orbits	Status of Data		Number of Lost Orbits
			Inconsistent	Missing	
1001	20	254-258	x		2
	22	270-274	x		4
	22	278-282	x		4
	22	282-287	x		5
	26	328-332	x		4
	28	353-357	x		5
	29	366-370	x		4
	30	370-374	x		4
	31	384-388	x		1
	31	388-391		x	3
1002	37	462-466	x		4
	43	537-541		x	4
1003	53	668-674		x	6
	54	684-689		x	5
1004	62	779-783		x	4
	64	804-813		x	9
	65	817-821		x	4
	75	946-950		x	4
1005	79	988-991		x	3
	87	1096-1102		x	6
1006	100	1255-1259		x	4
	104	1304-1309		x	5
1007	106	1334-1338		x	4
	110	1376-1380			
	120	1509-1513			
1008	125	1571-1576		x	5
	126	1580-1582		x	2
	136	1705-1709		x	4
1009	143	1798-1801		x	3
	145	1826-1830		x	4

TABLE 2 - continued

Tape ID	Julian Day	Orbits	Status of Data		Number of Lost Orbits
			Inconsistent	Missing	
1010	157	1973-1977		x	4
	168	2102-2105		x	3
1011	173	2173-2175		x	2
	182	2285-2289		x	4
1012	189	2371-2374		x	3
	192	2410-2415		x	5
1013	199	2503-2507		x	4
1014	218	2731-2737		x	6
	223	2798-2801		x	3
1015	230	2879-2884	x		5
	231	2891-2897		x	6
	234	2941-2947		x	6
	236	2960-2962		x	2
	238	2979-2991		x	12
	239	3004-3006		x	2
	241	3029-3035		x	6
1016	242	3041-3046		x	5
	244	3061-3063		x	2
	246	3080-3085		x	5
	248	3104-3110		x	6
	249	3117-3122		x	5
	249	3126-3129		x	3
	253	3167-3172		x	5
	253	3176-3179		x	3
254	3188-3197		x	9	
1017	257	3225-3228		x	3
	258	3238-3242		x	4
	261	3267-3272		x	5
	266	3335-3338		x	3
	268	3367-3373		x	6
1018	274	3439-3443		x	4
	279	3489-3492	x		3

TABLE 2 - continued

Tape ID	Julian Day	Orbits	Status of Data		Number of Lost Orbits
			Inconsistent	Missing	
	279	3498-3504		x	6
	280	3504-3505	x		1
	283	3542-3548		x	6
	285	3573-3576		x	3
	287	3598-3601	x		3
	288	3605-3611	x		6
1019	292	3655-3797		x	142
1020	304	3806-3810	x		4
	307	3849-3851	x		2
	309	3880-3882		x	2

Summary of Data Recovery

First Orbit - #231

Last Orbit - #3888

Total Possible Number - 3657 Orbits

61 Inconsistent Orbits

376 Missing Orbits

PREFLIGHT INSTRUMENT CALIBRATION

Several constants must be known in equations (2) and (3) before calculations of earth radiation parameters can be accomplished. These include the average broad-band absorptivities in equation (2), and long-wave emissivity, mass and case radiation constants in equation (3). All of these terms in the equations should be determined prior to launch and then checked thru inflight calibration procedures. However, in the case of the ESSA VII radiometers, the only preflight laboratory calibration which took place was enough data to determine the case radiation constants for the cone and plate radiometers. In addition to this information, data concerning the longwave optical properties of the black and white radiometers can be used to establish $\bar{\alpha}_L$ and ϵ .

Results of the investigation concerning the absorbing and emitting properties of the ESSA radiometers as well as the computation of the case radiation constants are presented in this section of the report.

LONGWAVE COLOR CONSTANTS

As a first approximation, the longwave absorptivities and emissivities are computed from theoretical models using available spectral absorptance measurements of the sensors' surfaces. It should be emphasized that these measurements may be somewhat different in absolute magnitude than the absorptance properties of the flight models. However, it is reasonable to assume that the gross variation of the absorptances with wavelength is similar; it is this variation that is being evaluated here.

Equations for computing absorptivities and emissivities are as follows:

$$\alpha_e = \frac{\int_{1\mu}^{50\mu} \alpha(\lambda) N(\lambda) d\lambda}{\int_{1\mu}^{50\mu} N(\lambda) d\lambda} \quad (4)$$

and

$$\epsilon = \frac{\int_{1\mu}^{50\mu} \epsilon(\lambda) B(T, \lambda) d\lambda}{\int_{1\mu}^{50\mu} B(T, \lambda) d\lambda} \quad (5)$$

where from Kirchoff's Law, $\epsilon(\lambda) = \alpha(\lambda)$. It is implicitly assumed here in the calculations that the observed spectral absorptances of each surface are valid for all temperatures of the detectors. This, in fact, may not be a valid assumption and should be investigated further.

When computing absorptances using equation (4), it is necessary to specify the variation of the earth flux with wavelength. A simple model is assumed which states that the variation in N occurs only in the atmospheric window region, between 8 and 13 microns. All other wavelengths emit at a constant temperature of 216.6°K which is the tropopause temperature of the Standard Atmosphere. This model grossly simulates the spectral emitting properties of the earth-atmosphere system. However, the results here agree with the correlation of nighttime plate observations presented later. In mathematical terms, this model states:

$$N(\lambda) = \begin{cases} B(216.6^\circ\text{K}, \lambda) & \text{for } \lambda < 8\mu \text{ and } \lambda > 13\mu \\ B(T, \lambda) & \text{for } 8\mu \leq \lambda \leq 13\mu \end{cases} \quad (6)$$

Calculations of the absorptivities and emissivities were performed for a variety of temperatures and simulated earth fluxes using equations (4) thru (6), and using the spectral absorptance data in Figure 4. The results of these calculations are presented in Figures 5 and 6 for the black and white radiometers, respectively. These results are plotted in terms of equivalent black body temperature which would correspond to the detector temperature in the case of emissivity, and the equivalent black body temperature for the longwave radiant exitance for the absorptivities. It is evident from these results that broad-band optical properties may vary significantly with temperature, even for the black paint. The uncertainties in this conclusion are the unknown variation of the spectral absorptances with detector temperature and the true character of the spectral absorptance curve beyond a wavelength of 25 microns. One certainty here is that proper calibration of the spectral properties of optical surfaces are important to the success of any future instrumentation such as the LZEEBE satellite system.

In order to process ESSA VII radiation data, some selection of longwave optical properties must be made from the information contained in Figures 5 and 6. In this regard, it is reasonable to select color constants for the nighttime and daytime mode of calculations. These selected values are presented in Table 3. It will be shown later that the selection of longwave color constant is consistent with nighttime observations (see section concerning correlation of plate and cone measurements).

POWER EXCHANGE BETWEEN RADIOMETER AND CASE

Preflight laboratory calibration data were available which provide information for determining case radiation constants for all radiometers

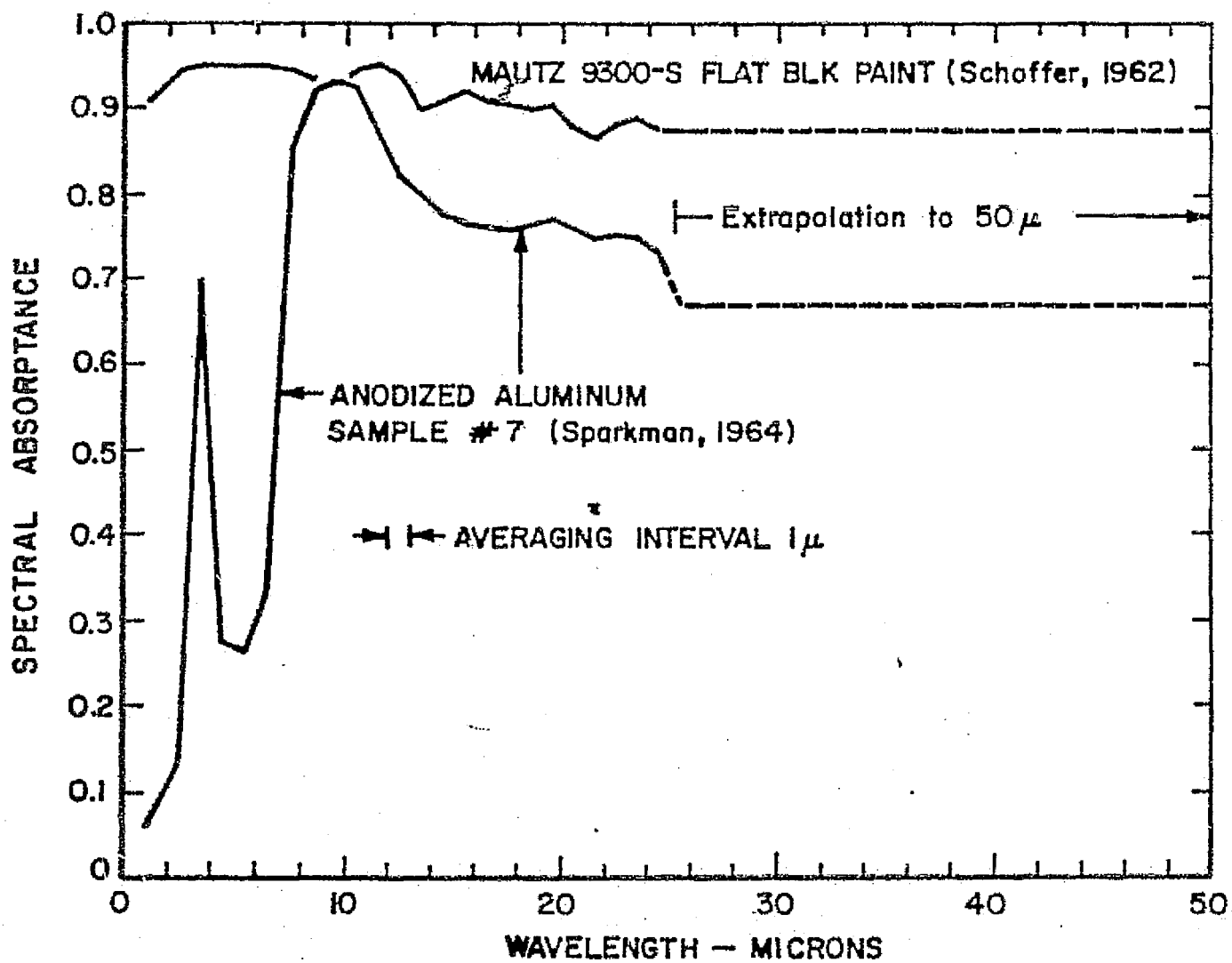


Figure 4. Spectral absorptance properties of the black and white ESSA radiometers.

MAUTZ 9300-S FLAT BLACK PAINT

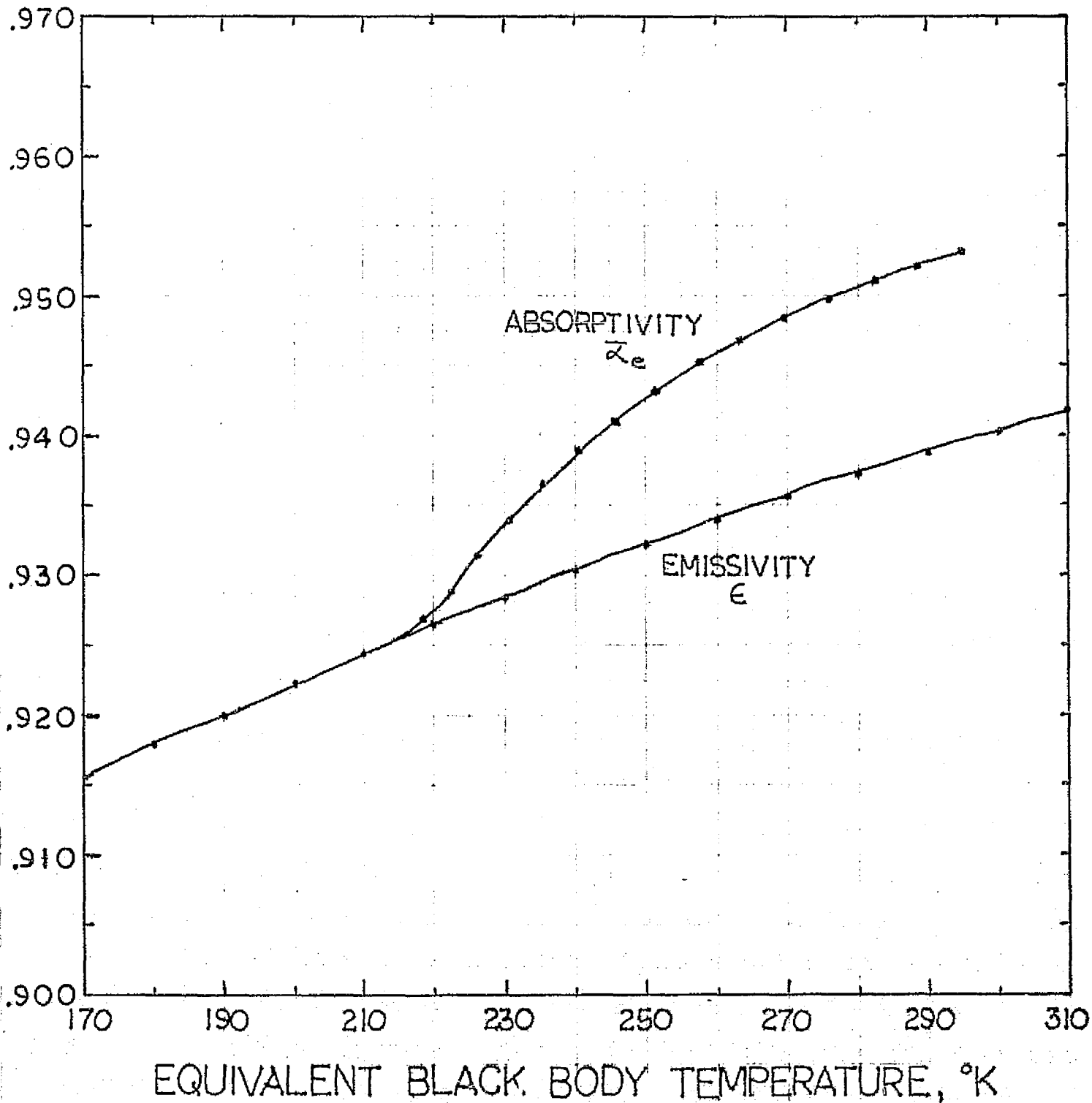


Figure 5. Variation in absorptivity and emissivity with temperature - black radiometers.

ANODIZED ALUMINUM SURFACE

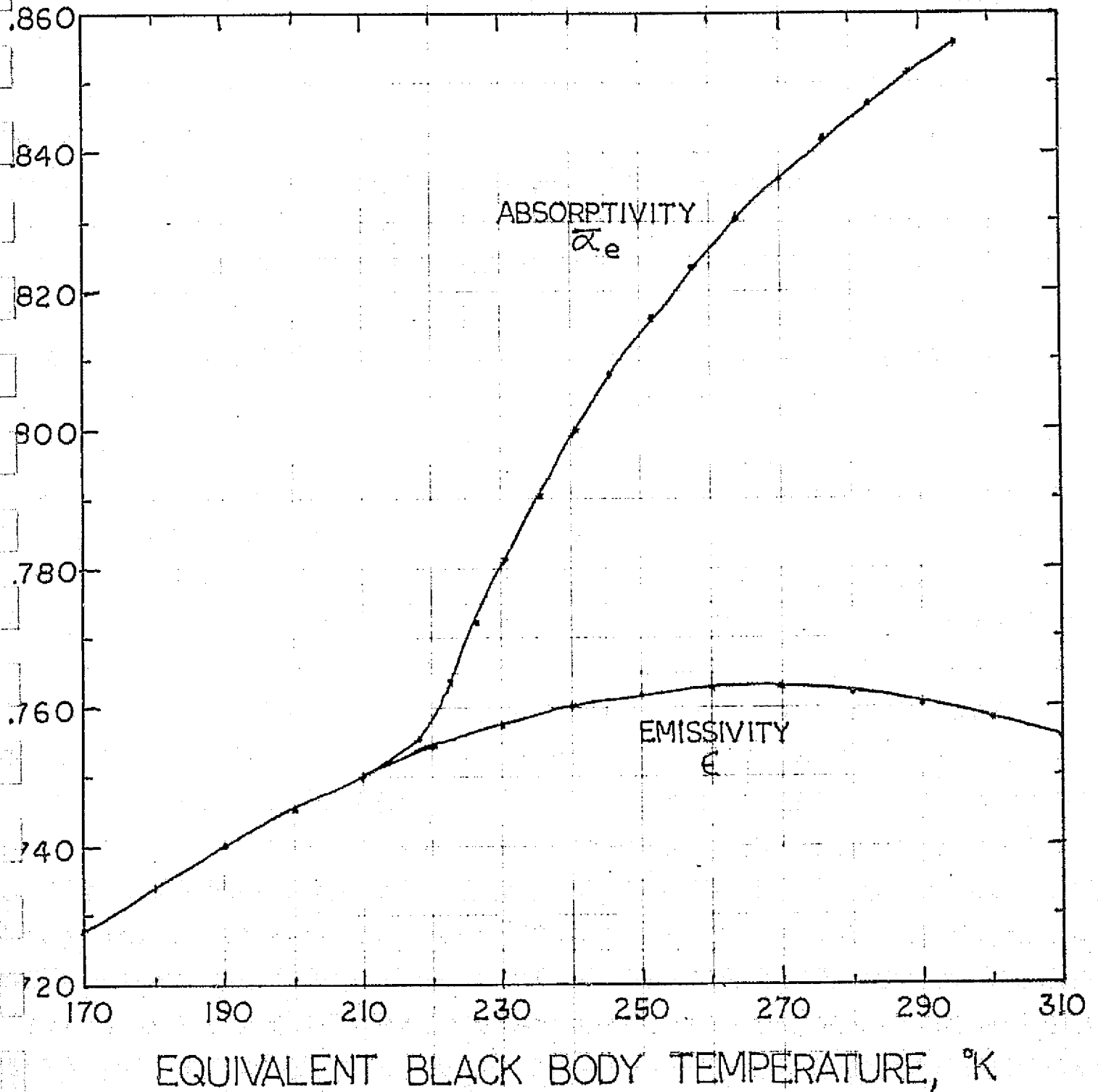


Figure 6. Variation in absorptivity and emissivity with temperature - white radiometers.

TABLE 3

Longwave Color Constants for ESSA VII Radiometers

Radiometer	$\bar{\alpha}_e$	Mode		$\frac{\epsilon_n}{\epsilon_d}$
		Nighttime ϵ_n	Daytime ϵ_d	
White Plate	.80	.74	.76	0.97
Black Plate	.94	.92	.94	0.98
White Cone	.80	.75	.75	1.00
Black Cone	.94	.93	.93	1.00

on ESSA VII. The calibration procedure consists of placing the flight version of the sensors in an enclosed vacuum chamber whose walls are maintained at a constant temperature. For all practical purposes, the chamber's surface is assumed to emit as a blackbody since its surface is painted black, and its area is large compared to the area of the sensor's surface. The chamber is maintained at a cold temperature (around -65°C) and its heat capacity is quite large compared to that of the sensor. Thus, the chamber maintains a known radiation field within the confines of the enclosure.

The sensor's case is heated electrically, and both the sensor and mount temperatures are monitored. These temperature data and the chamber temperature provide the available information for calibrating the sensor system.

The case radiation constant can be computed from an expression developed from equations (2) and (3). Since the radiant field within the enclosure is assumed to be black body radiation, the irradiance on the radiometers is σT_s^4 where T_s is the temperature of the source (i.e., the chamber). In radiative equilibrium, power lost by the radiometer back to the chamber is W_d . Equating these two components gives the expression

$$\frac{\bar{\alpha}_e}{\epsilon_n} \sigma T_s^4 = \sigma T_c^4 + R(\sigma T_c^4 - \sigma T_s^4) \quad (7)$$

Solving for the case radiation constant yields

$$R = \frac{(\sigma T_c^4 - \frac{\bar{\alpha}_e}{\epsilon_n} \sigma T_s^4)}{(\sigma T_c^4 - \sigma T_s^4)} \quad (8)$$

Incorporating longwave color constants listed in Table 3, calculations of case constants were performed using equation (8). The results of these calculations are presented in Table 4.

TABLE 4

Case Radiation Constants for ESSA VII Radiometers

<u>Radiometer</u>	<u>Case Constant R (no units)</u>
White Plate	0.075
Black Plate	0.054
White Cone	0.36
Black Cone	0.33

INFLIGHT CALIBRATION PROCEDURES

The previous section of the report discussed the determination of the longwave absorptivities and emissivities, and the case radiation constants for ESSA VII radiometers. Two parameters remain to be determined - the mass constants and the shortwave color constants. These parameters are best determined in the space laboratory where there is a hard vacuum and the best possible source of shortwave irradiance, the sun. The observational data themselves are used to determine the magnitudes of these parameters, utilizing the sun as a calibrating source of shortwave radiation.

The accurate determination of the shortwave color constants and the accurate monitoring of any changes in their values are of utmost importance to the confidence in ESSA VII data as well as the observational integrity of the LZEEBE system. This statement cannot be emphasized too many times. Therefore, every effort should be exerted to perfect the inflight calibration procedures.

Data utilized for these purposes are acquired during thermal transitions at ingress cool-down and egress warm-up of the radiometers exposed to direct solar radiation. At these particular locations of the satellite orbit, reflected earth radiation W_r can be neglected. Thus, the only sources of irradiation are H_s and W_e . If accurate calculations of W_e can be determined at times just before ingress and/or just after egress, it is possible to determine the radiometers' response to shortwave irradiance by subtracting the W_e magnitude from the observations. Thus, the radiometers can be calibrated, using the sun as the source, if the longwave earth term can be determined.

In order to perform the above shortwave calibration procedure, it is essential that the mass constants of the radiometers must be accurately known so that magnitudes of W_e can be calculated during thermal transitions. The goals then of inflight calibration procedures are to accomplish three things:

- * accurate measurement of W_e during thermal transitions.
- * frequent calibration of shortwave color constants.
- * periodic calibration of mass constants.

A considerable amount of effort was directed to this end, using ESSA VII data. Needless to say, several rather sophisticated approaches were tried but did not return good results. In the end, a simple approach turned out to be the best procedure. This approach is presented below.

CALIBRATION OF MASS CONSTANTS

Consider first the radiative balance equation just before ingress or after egress, i.e., calibration mode,

$$\frac{\bar{\alpha}_e}{\epsilon} F_e W_e + \frac{\bar{\alpha}_s}{\epsilon} F_s H_s = \sigma T^4 + M(T)\dot{T} + R(\sigma T^4 - \sigma T_c^4) \quad (9)$$

When the spacecraft passes into the earth's umbra, H_s is zero, and the equation takes on the form typical of nighttime calculations.

$$\frac{\bar{\alpha}_e}{\epsilon} F_e W_e = \sigma T_i^4 + M(T)\dot{T} + R(\sigma T^4 - \sigma T_c^4) \quad (10)$$

If the terms in equation (10) are arranged in the following manner where

$$\begin{aligned} \sigma T_i^4 &= \sigma T^4 + R(\sigma T^4 - \sigma T_c^4) \\ \sigma T_i^4 &= M(T)(-\dot{T}) + \frac{\bar{\alpha}_e}{\epsilon} F_e W_e \end{aligned} \quad (11)$$

This equation has the form of a straight line, $y = C_1 x + C_0$.

In this regard, the slope of the straight line C_1 is the mass constant and the intercept C_0 is the longwave earth term. This suggests that thermal transition data should be plotted on linear graph paper as σT_i^4 vs. $(-\dot{T})$. By analyzing the characteristics of this plotted function it is possible to establish the magnitude of the mass constant for the radiometer. Furthermore, changes in the slope of the function would suggest a variable mass constant.

Unfortunately life is not this easy. Implicit in the above discussion is the assumption that the longwave term $\frac{\alpha_e}{\epsilon} F_e W_e$ did not change during the thermal cool-down. This would be true if the satellite were stationary for about 6 minutes during cool-down. In real operation, low altitude spacecraft move about 1300 km ground track during this transition. As a general rule the earth term will not be constant during the acquisition of cool-down data. As a result, this will lead to distortions of the straight line equation discussed in equation (11). If a straight line were fit to the observed data through regression techniques, the functional distortions would manifest themselves in terms of slope changes.

In order to obtain a better understanding of the problem Luther (private communication) provided ingress cool-down data for a simulated LZEEBE balloon. The data are idealized in that the balloon has a uniform temperature at any time during thermal transition; however, his data are similar to measurements received from ESSA VII satellite. Three cases were analyzed with different longwave gradients during cool-down. In the control case, W_e was constant, i.e., $\dot{W}_e = 0$. In the other two cases, $\dot{W}_e = \pm 0.2$ (watts/m²)/sec.

The results of the analysis of simulated balloon data are presented in Figure 7 where the normalized radiant power is plotted as a function of $(-T)$. It is evident from this plot that the data where the longwave earth term was constant appears as a straight line. When there is a significant gradient in the earth term the function is concave downward for $\dot{W}_e < 0$, and concave upward for $\dot{W}_e > 0$. In other words, longwave gradients during cool-down distorted the linearity of the function. In addition, the average slopes of the functions increased for $\dot{W}_e < 0$, and decreased for $\dot{W}_e > 0$. Analysis of simulated data such as this was a tremendous help in understanding observations from ESSA VII satellite.

Based upon these results, it was decided to filter the cool-down data from ESSA VII and select only those cool-down functions which exhibit linearity. In fact, such a linearity criterion could be incorporated in the electronics logic aboard the spacecraft in order to select useable calibration data. These data selections were further verified by examining the cone temperature data during the same temperature transitions.

A similar procedure as outlined above can be followed in analyzing warm-up data during satellite egression. For these data, the variable term affecting functional linearity is still associated with longwave earth radiation. There is also a large constant associated with direct solar irradiation (see equation 9), which results in a large value for the intercept value C_0 in a curve-fit of the data. The slope of the line in a linear curve-fit of the egression is still related to the mass constant.

A selection of data was taken from filtered ingress and egression cases throughout the 10 month period of ESSA VII measurements.

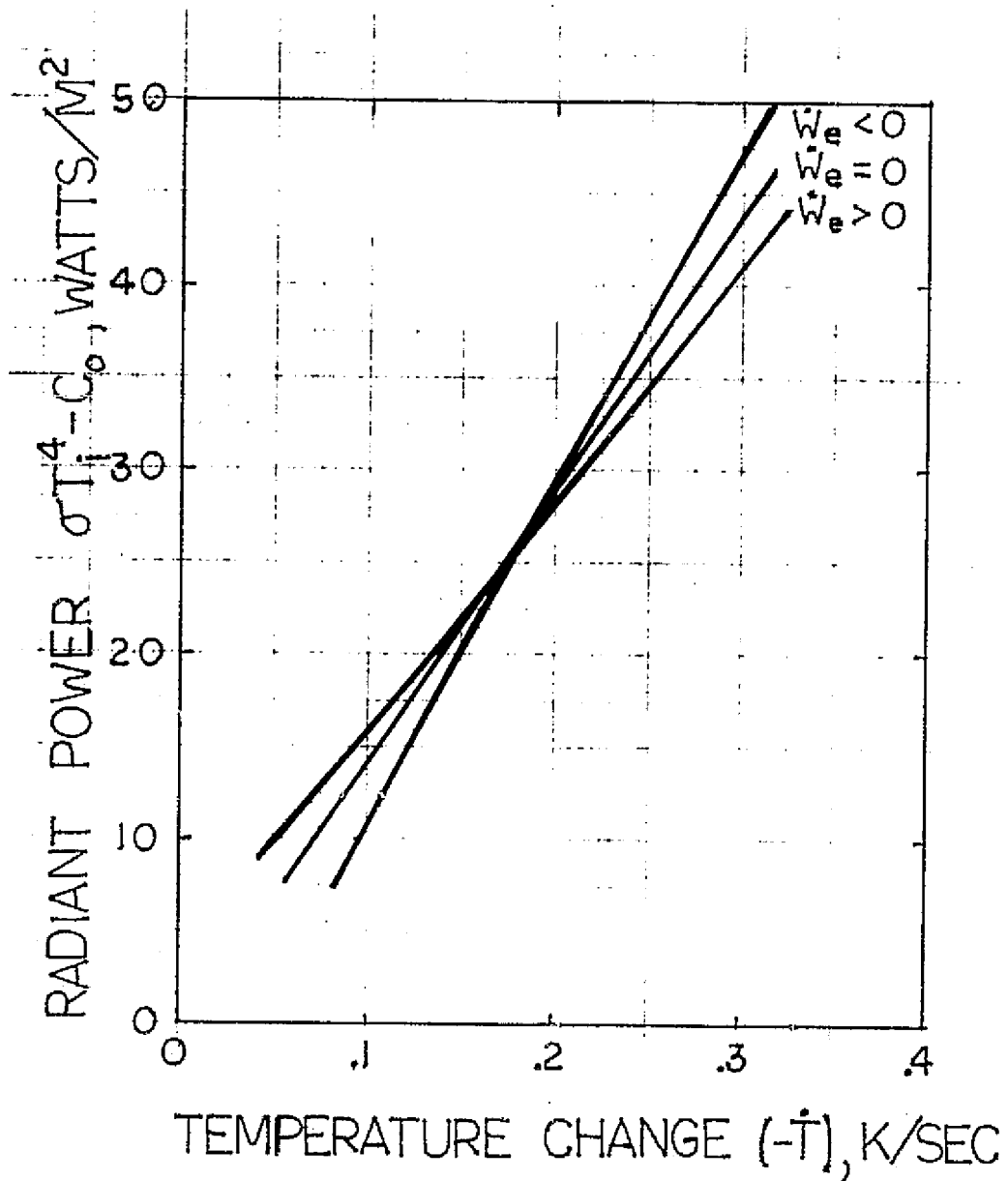


Figure 7. Simulated ingress data for a LZEEBE balloon radiometer.

Each of these cases was fit with a straight line, and then the data were plotted on one graph in a normalized fashion as shown in Figure 7. Ingression and egression data were treated separately.

A detailed study of the data showed that a smooth curve drawn through the mass of points still exhibited a change in slope during both the cool-down and warm-up transitions. This change in slope is attributed to a variable mass constant. A cross plot of T vs. \dot{T} was generated from the data in order to relate the variable mass constant in terms of radiometer temperature. The results of all this effort are presented in Figure 8 where the mass constants are plotted as functions of plate temperatures. As can be seen from the graphs, the mass constants are no longer constant, but linear variables increasing as a function of radiometer temperature. A more appropriate name for $M(T)$ might be the "mass term."

The uncertainties of each of the points are indicated in Figure 8. The vertical uncertainty in mass term magnitude is based on the ability to determine the slopes of the ingression - egression data discussed in the previous paragraph. The horizontal uncertainty in temperature is based on the scatter of points in the cross plot of T vs. \dot{T} .

It should be mentioned here in a historical sense that there were several fruitless attempts to determine any significant variations in the mass constant as a function of temperature. The key to the solution of the problem was data filtering, i.e., selecting only those cases that exhibit linearity and thus some assurance that the longwave earth radiation term was constant during thermal transitions.

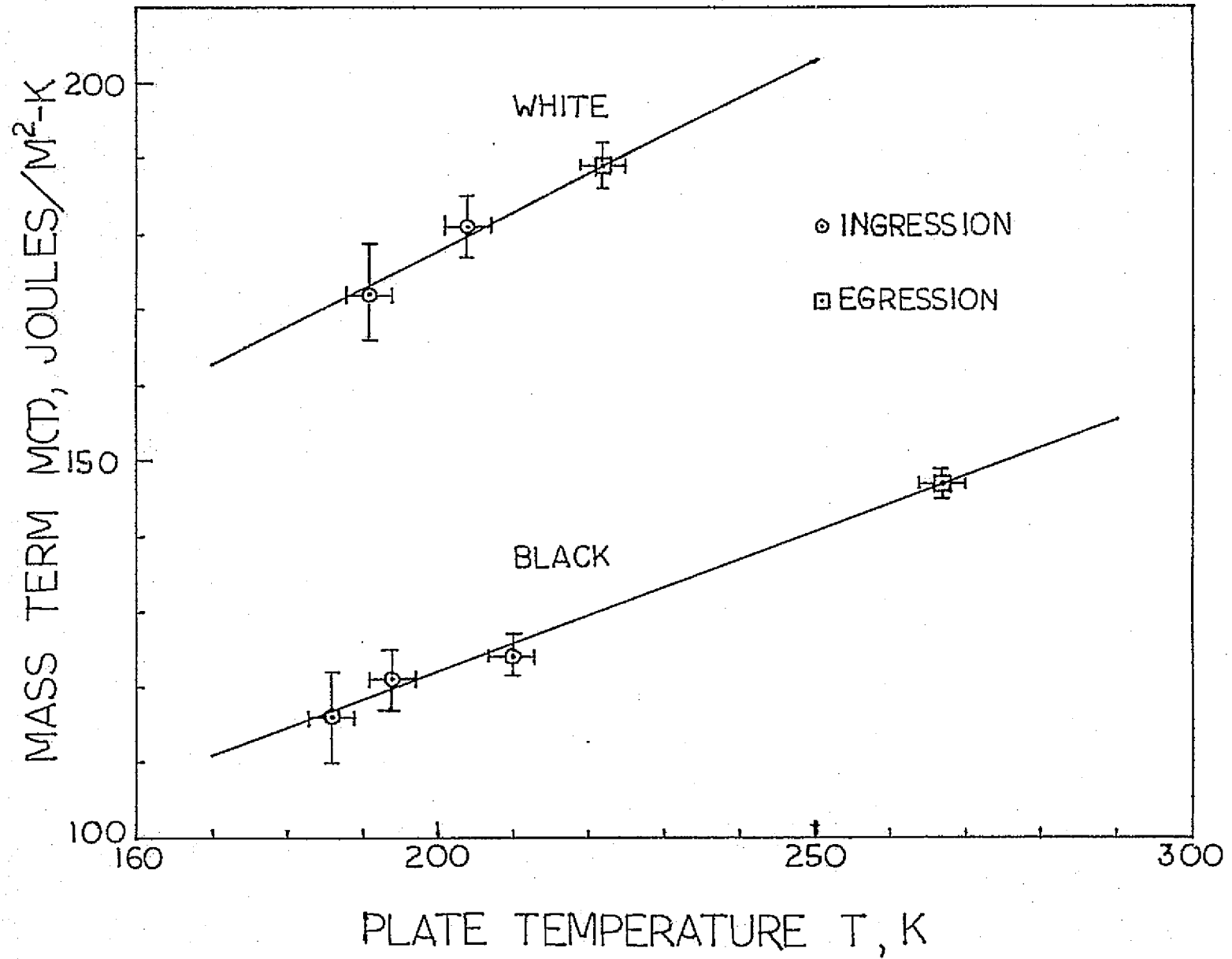


Figure 8. Variation in mass term with temperature for the white and black radiometer

CALIBRATION OF SHORTWAVE COLOR CONSTANTS

The problem of calibrating shortwave color constants rests primarily on the ability to calculate accurate longwave earth terms $\frac{\alpha_e}{\epsilon} F_e W_e$ during the thermal transition. Since accurate values of the mass term were established in Figure 8, it follows that accurate values of the shortwave color constants can be calculated.

During the course of this portion of the investigation, numerous, sophisticated approaches were attempted with little results. After a careful examination of the failures of other approaches, the simplest of procedures seemed to work best.

The concept of the procedure is presented in Figure 9. The solid points are the radiant power densities associated with an ingress cool-down of the black plate on ESSA VII. The assumed time of ingress is indicated on the graph. There is a two minute time interval following this time which is a period of solar contamination, i.e., the sun's disc is setting beneath the viewed horizon of the earth at satellite altitude. This time period is associated with the penumbra of the earth's shadow. Before this period daytime mode calculations are appropriate (see equation 9) - after this period, nighttime mode calculations are used (see equation 10). The middle time of this 2 minute period is defined as the time of calibration (see t_c at the bottom of Figure 9).

The last four daytime mode calculations (first four solid points on graph) are used to extrapolate the trend of observations forward in time over a one minute period to the time of calibration. In a similar manner, the first four computed longwave earth terms (see first four open points at bottom of graph) are used to extrapolate the trend line of the longwave

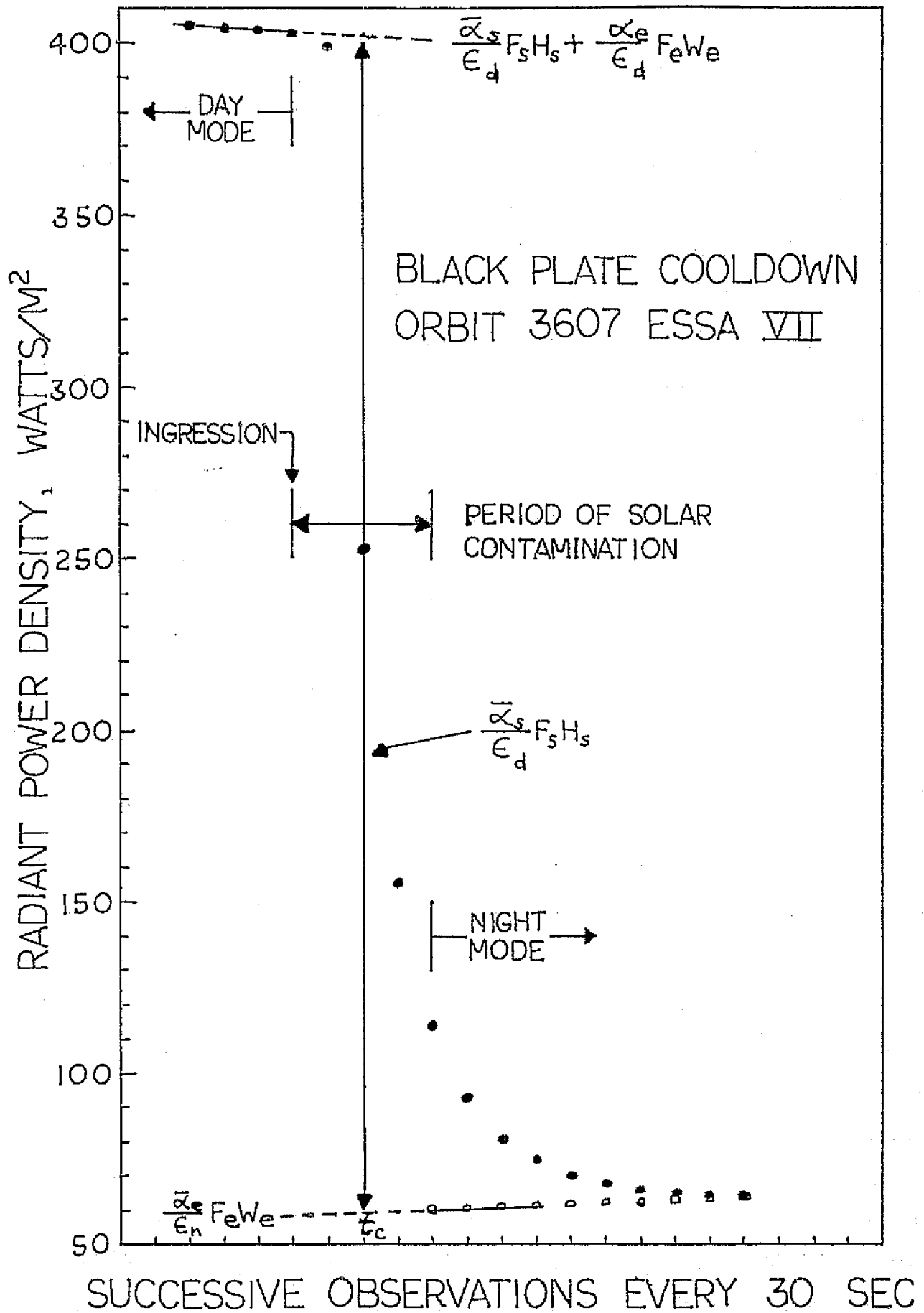


Figure 9. Concept of shortwave color constant calibration procedure.
(see text for description)

term backwards in time to the time of calibration. The computed magnitudes of these two trend line extrapolations at the precise time of calibration are subtracted from each other. The resulting magnitude of radiant power density constitutes the response of the black plate solely to direct solar irradiation. In the example shown in Figure 9, the following magnitudes arise from this procedure:

$$\frac{\bar{\alpha}_s}{\epsilon_d} F_s H_s + \frac{\bar{\alpha}_e}{\epsilon_d} F_e W_e = 402.5 \text{ watts/m}^2$$

$$\left(\frac{\epsilon_n}{\epsilon_d} \right) \frac{\bar{\alpha}_e}{\epsilon_n} F_e W_e = 59.3 \text{ watts/m}^2$$

Thus, the solar term becomes

$$\frac{\bar{\alpha}_s}{\epsilon_d} F_s H_s = 343.2 \text{ watts/m}^2$$

The solar term is indicated on the graph in Figure 9 at the time of calibration.

The above procedure works even better for egression warm-up data . since the radiometer approaches an equilibrium temperature more rapidly than in the case of cool-down.

Determinations of the solar term from consecutive cool-down, warm-up thermal transitions indicates differences of magnitudes of less than one watt/m² on the average. Good agreement such as this leads one to have confidence in the shortwave calibration procedure and in the determination of mass constants.

ANALYSIS OF ERRORS

The question always arises as to the accuracy of the inflight calibration procedures. This pertains to both the absolute accuracy of the cali-

brations as well as determining the change in the solar terms of each radiometer. It should be pointed out that the absolute temperature accuracies of the observations are not considered in the evaluation of the calibration procedure since they are assumed to be correct.

Without question, the accuracy of the inflight calibration procedure depends on the accurate determination of the mass term in Figure 8. Within the uncertainties of the points plotted on the graph, one can determine a radically different change in mass term with temperature simply by changing the slope of the line, and still remain within the uncertainties indicated. However, such a change will produce inconsistencies in the solar terms between ingress and egress thermal transitions. Thus, it is possible to set the slope of the mass term change with temperature with some certainty, based solely on inflight data.

Another aspect of the evaluation of the curves in Figure 8 which pertain to calibration accuracies is the translation of the curve up or down, a bias change, without affecting the slope of the curve. This adjustment truly affects the absolute accuracy of the solar term observations within the uncertainty of the points on the graph. This uncertainty amounts to ± 2 mass term units for the black plate and ± 3 units for the white plate. This uncertainty results in about a ± 1 watt uncertainty in the solar terms of each of the plate radiometers. The only way to reduce this error is to consider hundreds of cases in order to drive down the random uncertainty of the mass term determinations. Such an approach is certainly feasible.

When one considers other errors related to the accurate determination of shortwave and longwave earth fluxes such as the spatial sampling problem, the evaluation of shape factors for the anisotropic reflection problem, and the assumption of constant broad-band absorptivities, one quickly concludes that these problems are larger in magnitude than the errors associated with inflight calibration of shortwave color constants. It is estimated that these other problems are in the one to two percent error range, whereas, the inflight calibration uncertainty on the order of one watt/m², or a few tenths of a percent error.

It is concluded from the discussion in this section of the report and from the investigation of the inflight calibration problem that valid shortwave calibrations can be obtained solely from inflight data with a sampling frequency every 30 seconds.

CORRELATION OF PLATE AND CONE MEASUREMENTS

Correlations of plate and cone measurements during nighttime mode operation give considerable insight as to the relative longwave optical characteristics of the radiometers. During the nighttime mode, the pair of plate radiometers, and the pair of cone radiometers view identical longwave irradiance fields. By imposing this boundary condition, it is possible to evaluate the relative $\bar{\alpha}_e/\epsilon$ ratios of the white and black optical surfaces.

In a similar manner, correlation of plate and cone measurements give information concerning the relative geometrical viewing properties of the two radiometer types. It must be remembered in the latter case, however, that the cones absorb longwave irradiance from a restricted portion of the earth viewed area. Thus, the boundary condition that the cones and plates view the same irradiance field does not hold exactly, but is a reasonable approximation for the mean of many observations.

Correlation of plate and cone measurements from ESSA VII were performed during this investigation for many observations throughout the ten month period of useful satellite data. Typical correlations for a selection of these data are shown in Figures 10 and 11.

The correlation of the white plate radiometer with the black plate radiometer is shown in Figure 10 where the white power density is plotted on the ordinate vs. black power density on the abscissa. By plotting the measurements in this manner, the slope of the linear regression line through the points is equal to the ratio of $\left(\frac{\bar{\alpha}_e}{\epsilon}\right)_{\text{white}} / \left(\frac{\bar{\alpha}_e}{\epsilon}\right)_{\text{black}}$. The slope of the line for the data in Figure 10 indicates a magnitude of (1.06).

CORRELATION OF NIGHTTIME PLATE OBSERVATIONS

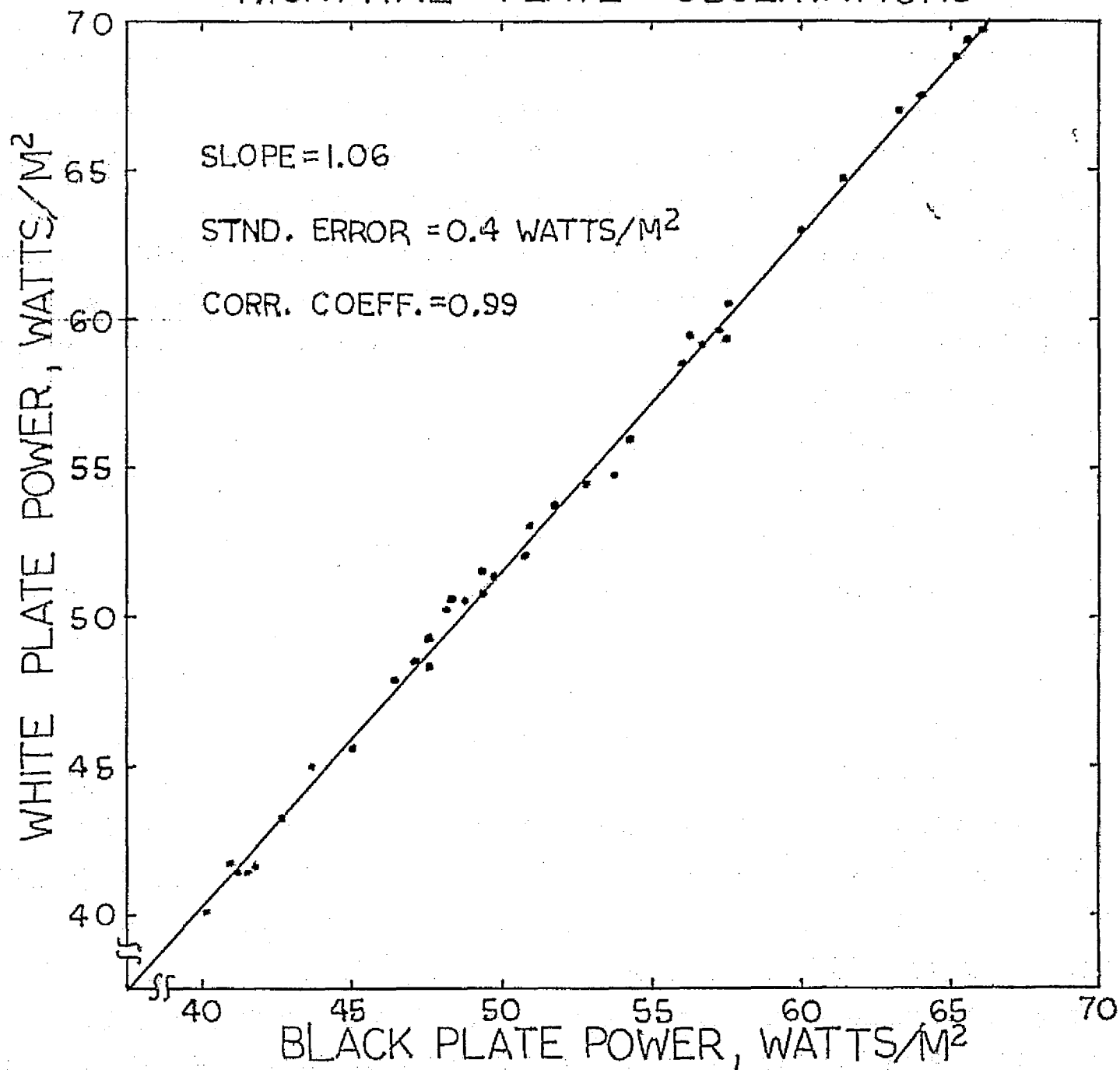


Figure 10. Correlation of white plate vs. black plate radiometers

This result suggests that the $(\bar{\alpha}_e/\epsilon)_w$ ratio of the white plate is roughly 6 percent larger than a similar ratio for the black plate. Referring to the values of longwave optical properties presented in Table 3, the computed ratio for white vs. black plate, using nighttime values, is 1.058 in magnitude, in good agreement with the correlation of nighttime observations presented in Figure 10. Thus, one has confidence in the longwave optical properties developed in the section on preflight instrument calibration, even though a crude model was employed for the upwelling spectral irradiance from the earth.

It is noted further from the correlation in Figure 10 that the standard error of the estimate is 0.4 watts/m^2 , that is, about 68% of the points fall within $\pm 0.4 \text{ watts/m}^2$ of the line. In order to interpret this result in terms of W_e earth flux values, a multiplier of approximately 4 is appropriate, giving a $\pm 1.6 \text{ watts/m}^2$ standard error. This magnitude of uncertainty is rather large, about 0.7% of the average W_e magnitude. In fact, this uncertainty is larger in magnitude than the errors in the solar terms of each radiometer discussed in the previous section. The reason for this uncertainty is the point to emphasize here. It is due to the fact that the spectral absorbing properties of the optical surfaces are not uniform across the longwave, broad-band spectrum. This point is easily understood by considering the observed spectral absorptance properties of the anodized aluminum "white" sample shown in Figure 4.

As mentioned earlier in this section, the correlation of plate and cone measurements gives information concerning the relative geometrical viewing properties of the two radiometer types. In this regard, it is assumed that the optical properties of the black paint or anodized aluminum surfaces are

the same - certainly a reasonable assumption. An example of this correlation is presented in Figure 11 where the black plate observations are plotted as a function of concurrent black cone radiant power densities. A linear regression line was computed for these data, in a manner similar to the results in Figure 10. The slope of this line has a different interpretation than in the plate correlation. The slope is related to the ratio of shape factors for the plate and the cone radiometers, i.e., $\text{slope} = (F_e)_{\text{plate}} / (F_e)_{\text{cone}}$. This ratio is 0.72 for the data shown in Figure 11.

The results in Figure 11 have further engineering design implications concerning the LZEEBE system. The standard error of the estimate for the data shown in Figure 11 is $\pm 1.1 \text{ watts/m}^2$. When this uncertainty is interpreted in terms of W_e , a variation of about $\pm 4.4 \text{ watts/m}^2$ is obtained. Similar uncertainties were obtained in a prior study by House (1968) when he correlated the change in plate observations vs. the corresponding change in cone observations, utilizing ESSA III data. This magnitude of uncertainty is greater than 1% of the W_e irradiance field. Therefore, it is concluded that auxiliary, longwave gradient detectors would not have significant value in defining the longwave earth term during inflight calibration of shortwave color constants. In fact, the error in the plate - cone correlation is larger than the uncertainty in the inflight calibration procedures developed in the last section.

STUDY CONCLUSIONS RELATED TO LZEEBE SYSTEM CONSIDERATIONS

An attempt should be made here at the end of this report to summarize the conclusions of the investigation and how these conclusions relate to the engineering design and flight operation of the proposed LZEEBE system.

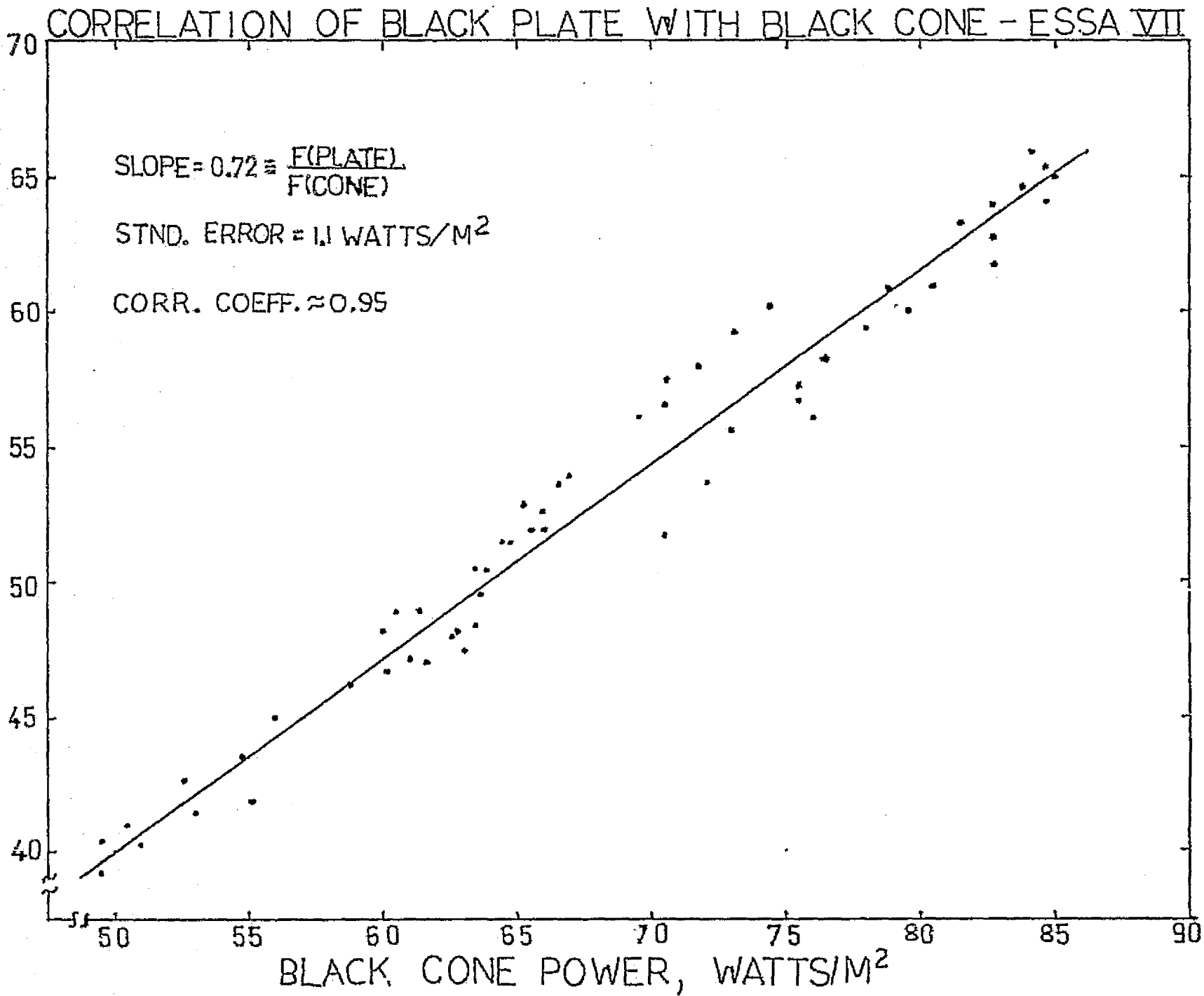


Figure 11. Correlation of black plate vs. black cone radiometers.

It may be recalled that the major objective of this effort was to obtain ESSA VII raw data and process it to a point where it can be further analyzed for the development of long-term earth energy experiments and documentation of climate trends. It is felt that this objective was accomplished during the reporting period. Data recovery during the 10 month observation period of ESSA VII was about 90% efficient. Certainly there is an abundance of useable observations for future investigations. Data are stored on 20 reels of computer tape in a FORTRAN readable format.

A considerable amount of effort was spent in developing successful preflight and inflight calibration procedures for determining critical constants required for the future calculation of radiation balance parameters. Even though these procedures pertain to ESSA VII radiometers they find direct application to the balloon radiometers of the LZEEBE system. In some ways the ESSA VII data reduction problem is more complicated than that for the LZEEBE system since a spinning flat plate has a more complicated geometry than an omni-directional sphere.

Specific conclusions of this study and their relationship to engineering design and flight operations of the LZEEBE system are outlined below:

ENGINEERING DESIGN CONSIDERATIONS - LZEEBE SYSTEM

Optical Constraints

- detectors should have uniform spectral response to both the shortwave and longwave broad-band spectral regions.
- knowledge of the spectral absorbing properties of optical surfaces must be known between about 0.2 microns to about 50 microns or longer wavelengths, if possible.
- the variation in spectral absorbing properties must be known for the expected ranges of radiometer temperatures and for the above spectral region.

- white optical surfaces like anodized aluminum and teflon
- backed with aluminum have inferior longwave optical properties compared to paint binders.

- white paints with binders similar to the black paints may
- be preferred to the above materials provided the shortwave optical degradation is not too severe.

Geometrical Constraints

- knowledge of the angular absorbing properties of the optical surfaces with wavelength is desirable to develop accurate geometric shape factors.

- optical surfaces should be exposed to direct solar irradiance uniformly, if possible, so that any changes in optical properties will be the same over the balloon's surface area.

Other Considerations

- crude longwave gradient detectors will not provide the needed accuracies of earth radiation gradients during thermal transitions - however, these detectors may be useful in determining rough satellite orientation to solar radiation.

- all physical and optical properties of the balloon radiometers should be known prior to launch - this enhances the value of inflight calibration results.

FLIGHT OPERATIONS - LZEEBE SYSTEM

<u>Type of Observation or Calibration</u>	<u>Data Sampling Time Interval</u>	<u>Time Frequency of Performance</u>
W_e and W_r (daytime mode)	30 to 120 sec	30 to 120 sec
W_e (nighttime mode)	30 to 120 sec	30 to 120 sec
W_e (calibration mode)	30 sec	30 sec
Mass term calibration $M(T)$	30 sec	all orbits - analyze filtered orbits
Calibration of solar term ingress & egress $\left(\frac{\alpha_s}{\epsilon} F_s H_s\right)$	30 sec	all orbits - analyze filtered orbits
Albedo calculation A	system independent (use W_r averages)	over time period of data analysis
Calibration $F_s H_s \left[\begin{pmatrix} \alpha_s \\ \alpha_e \end{pmatrix}_a - \begin{pmatrix} \alpha_s \\ \alpha_e \end{pmatrix}_b \right]$	30 sec	all orbits - cross check with solar term calibrations

REFERENCES

- Bignell, K. J., 1962: Heat balance measurements from an earth satellite - An analysis of some possibilities. Roy. Meteor. Soc., 231-244.
- House, F. B., 1965: The Radiation Balance of the Earth from a Satellite. Ph.D. Thesis, Department of Meteorology, The University of Wisconsin.
- _____, 1968: The reduction, analysis and interpretation of radiant flux measurements from ESSA weather satellites. Final Report under ESSA/NESC Contract No. E-108-67(N), GCA-TR-68-20-G, GCA Corporation, Bedford, Massachusetts.
- _____, 1970: The reduction, analysis and interpretation of radiation balance measurements from ESSA Weather Satellites. Final Report under ESSA/NESC Contract No. E-119-68(N), GCA-TR-69-17-G, GCA Corp., Bedford, Massachusetts.
- _____, G. Sweet, et.al., 1973: Long-term Zonal Earth Energy Budget Experiment (LZEEBE). A proposal to AAFE, April.
- Luther, M., 1974: Private Communication
- MacDonald, T., 1966: Unpublished seminar presented in November at the Department of Meteorology, The University of Wisconsin, Madison, Wisc.
- Möller, F. and E. Raschke, 1969: Problems of meteorological observations from satellites. Space Science Reviews, Vol. 9, No. 1, 90-148.
- Nelson, D. F. and Parent, R., 1967: The prototype flat-plate radiometers for the ESSA III satellite. Annual Report on Grant No. WBG-27, Department of Meteorology, The University of Wisconsin.
- Suomi, V. E., 1958: The Radiation Balance of the Earth from a Satellite, Annals of the IGY, VI, 331-340.
- _____, 1961: The Thermal Radiation Balance Experiment on Board Explorer VII Satellite, NASA Tech. Note D, 608.
- _____, Hanson, K.K., and Vonder Haar, T. H., 1967: The theoretical basis for low-resolution radiometer measurements for a satellite, Annual Report on Grant No. WBG-27, Department of Meteorology, The University of Wisconsin.
- Vonder Haar, T. H., 1968: Variations of the Earth's Radiation Budget. Ph.D. Thesis, Department of Meteorology, The University of Wisconsin.
- Weinstein, M. and Suomi, V., 1961: Analysis of satellite infrared radiation measurements on a synoptic scale. Monthly Weather Review, 89, 419-428.

APPENDIX A

COMPUTER SOFTWARE FOR PRELIMINARY PROCESSING
OF ESSA VII SATELLITE DATA

DESCRIPTION OF THE MAIN PROGRAM

A two block approach is used in the processing of all data. The main program calls the input procedure and it is from there that all of the data is read in. Data is read from the CDC tapes one block (25 lines) at a time and assembled into the two arrays ORBIT and SENSOR. These two arrays are then passed back into the main program. There are always two blocks of data in storage at any one time. Differences in angles and count values are computed in order to perform the necessary counts to temperature conversion, and as the last lines of each block are processed some overlap into the next block is necessary. Upon completion of all work on a block, that block (consisting of the finished ORBIT and SENSOR arrays) is written onto tape and the next block of data is read in. This approach reduces the total amount of time needed since computations on each block are being performed at the same time that the previous block is being written. Parts A and B of the main program segment are therefore identical and control is passed to either part depending upon which particular block is being processed.

The first loop in PARTA (down to label PHILA) determines the day-night position of the satellite and adds 1024 counts onto the black plate day-time count values. Bad rows are skipped. The satellite position logic is as follows. The principle testing point was the zenith angle (column 5 of ORBIT array). Experience showed that the day-night transition occurred within a window of zenith angle values ranging roughly from 120 to 128 degrees, with the angle increasing in going from day to night and decreasing from night to day. If the zenith angle was less than 115 degrees, daytime was assumed, and 1024 counts were added onto the black plate values. All other lines with zenith angles greater than 115 degrees were subject to

further testing. Ensuing tests required 1) the sense of direction of the zenith angle (either increasing or decreasing) and 2) the gradient of the black plate count values. Actual processing indicated the need for one additional test because in some readouts bad data occurred in the transition zone and the change from day to night (or vice versa) was not detected. A third variable was computed, the absolute difference between the black and white plate count values. These two values agree quite well during the nighttime observations and they differ greatly in daylight. If this difference was less than 100 counts then night was assumed. Finally, if white plate counts ran greater than 350, then daytime was assumed. On testing any one good line of data, if the succeeding line contained a black plate count value of 9999 then the line being tested was replaced with 9999 since the black plate gradient and other variables could not be computed. This results in the loss of some good data but the generally good condition of the data makes this loss negligible. The program segment from the label PHILA to the label IOWA performs all of the above operations using the last lines of one block and the first lines of the succeeding block. The segment from the label IOWA to the label ELM works on the first column of SENSOR array which contains the reference resistor count as well as the mount count values. Again bad data lines are skipped and since the count values of these sensors do not fall below 400 any values below 400 have 1024 added to them. The segment from label PBY to label ILL converts count values to temperatures for the black and white plates and cones. All count values are adjusted using the reference resistor count (all counts are multiplied by .994 for ESSA 7). Since the temperature tables had to be split into two parts of 1000 and 500 lines, count values had to be tested and converted to temperatures using the appropriate table. In order to

safeguard against a stoppage in program execution due to negative count values (count values are a parameter of the temperature table arrays) any count values exceeding the acceptable limits were automatically set to a value of 500. This would effectively place a temperature of 0.00 at that location. An inspection of the temperature tables shows that no temperature of exactly 0.00 can exist in the data. Therefore, in performing any additional processing of this data a test for zero temperatures on all seven sensors should be made. Appearance of these zero values will indicate original data which were out of the temperature tables range. The program segment from label TEX to label NH uses the above procedures to convert mount count values to temperatures. The remaining lines from label NM to label PARTB write the finished data onto tape, write end of file on tape, increments the record counter, and reads in a new block of data via an input statement. PARTB comprises the rest of the program and is identical to PARTA.

INPUT PROCEDURE DESCRIPTION

The input procedure is used to read in new data from the input tapes, screen the data, and set up the ORBIT and SENSOR arrays which are passed back into the main program. The twenty eight work documentation headings as well as most of the end of files are also written onto the output tape from this procedure. When a readout is finished and an end of file written, the record counter in the main program is set to zero and the input procedure is called again. There are two read statements in this procedure labelled MINN and ONT respectively. MINN is executed when the record counter is zero and it is used to read in the initial input files consisting of the twelve word label as well as the twenty eight word documentation headers. Upon writing the twenty eight word heading control is passed back to the main program, the record counter is incremented, and the

input procedure is called again. Now data will be read in from the read statement labelled ONT as long as the record counter is not zero. Also notice the two statements before the label ONT. These two statements effectively skip the first twenty five lines of each readout (when REC=1) for reasons which are stated later. The program segment from the label MINN to the label THRTY is probably the most difficult part of the entire program. As end of file and parity problems were encountered, it was necessary to revise this section continually. The logic shown is a combination of that which was needed for routine execution of the program and that which was needed to cover any abnormalities which arose. Initially, the final twenty five line record of each readout was partially filled with anywhere from five to twenty five lines of data (in groups of five lines) while the rest of the lines in the record were filled with zeros (it was possible for this last record to be completely filled as it turned out). This incomplete record was being used initially to indicate the end of a readout but the program was eventually modified in order not to rely on this. As a result of the change though, the last partially filled record of each readout was not written onto the output tape. The third line before the label OAHU checks the satellite height. If zero, this would signal the end of a readout. The variable X would be set to one and this variable along with E would be passed back into the main program where it was tested. The segment from the label OAHU to the label FIVE sets up the ORBIT array, checking the condition of each line of data and replacing bad lines with 9999. The loop from label FIVE to label SIX sets up the black and white plates and cones data in the SENSOR array, and subtracts 1024 from any count values which are greater than 1024. The loop from the label MAUI to the label SSP performs the same operations for the mount counts and the refe-

rence resistor count. The next program segment from label SSP to label OKLA was a later addition to the program. Errors in time were detected and they showed up in the zenith angles of the day night transition zones. These errors were found to cause as much as a nine degree discrepancy in the subpoint latitude. This made it necessary for every readout to be checked for this problem. As stated, Record one of each readout is always skipped since experience showed that data in this record were often ill conditioned and were eliminated anyway. It was decided to allow the mechanics of the data system settle somewhat, before this time testing would be performed. As a result, Records three thru nine were tested for this possible error in time. These seven records yield 175 lines of data and this corresponds to approximately 85 minutes of orbit time. In checking for this error, particular attention is paid to the transition zones and one of the tested records will most certainly contain such a zone. Specifically, the test is as follows. If the zenith angle (called D in this segment) is less than 119 degrees then the satellite should be in the sun. White plate counts should then be greater than 350. If these counts are less than 350 a time error is indicated along with the record number where it was detected. This indication appears in the printed output log. The file is immediately closed on the output tape and the rest of the readout is skipped. If the zenith angle is greater than 132 degrees then the satellite should be in darkness and again the white plate counts are tested. Here, if these count values are greater than 350 a time error is recorded as before. Since this test had to be added to the program, partial readouts now occur on the output tapes. These partial readouts can be skipped by noting the skipped orbit numbers in the printed log and then bypassing these orbits during further data processing. In a very general way, this is all

that the input procedure does. The remaining segments of the procedure are composed of the end of file and parity action labels. There is only one remaining test to be discussed. Tape number 16 of the ESSA 7 series contained a readout consisting of approximately one 25 line record. A test was devised which would determine approximately how far along into the data the program had progressed. It was necessary to determine rather roughly the orbit number of the last readout on each tape. This can be done rather easily if the satellite launch date as well as the beginning and end date of each tape are known. For the ESSA 7 tapes these dates were written on each of the input tape boxes.

BEGIN

FILE FILES 12 "TTABIE" "PH3144" (2,10,150);
FILE LINE 1(2,17);
FILE T 9(1,375);
FILE BT 2 "PH3144" (1,350,SAVE 90);
FORMAT FMT1 (15,718.2);

FORMAT FMT10 (" RECORD EQUALS "*,15);

FORMAT FMT4(14F9.2);

INTEGER REC,X,L;
INTEGER H;
REAL U,V;
REAL DELTAF,DELANG,DELTAI;
ARRAY ADMBIT,BURBIT(0:24,0:6),ASENSOR,HSENSOR(0:24,0:5);
DEFINE THRU= STEP 1 UNTIL#;
DEFINE STIB=(IF SH THEN DS+RESET ELSE DS+SET; SKIP 1 SH);
DEFINE BITS=(IF SH THEN DS+SET ELSE DS+RESET; SKIP 1 SH);
DEFINE THINGS=3,1#;
DEFINE KEY="3"//777//77700505"##;

STREAM PROCEDURE RESTRING(A,B,FK);
BEGIN
LOCAL J,K;
SI(4) DI(4); K(0); DI(4);
I(0) (J(0)); DS+RESET;
IF SH THEN BEGIN
DS+SET; DI(K); DI(0)+6;
12 STIB; K(0); DI(J);
SKIP 2 DB;
DS+7 RESET; 39 SITH;
END ELSE
BEGIN
DS+RESET; DI(K); DI(0)+6;
12 BITS; K(0); DI(J);
SKIP 2 DB;
DS+7 RESET; 39 BITS;
END;
SKIP 9 SJ);
END RESTRING;

ORIGINAL PAGE IS
OF POOR QUALITY

```

STREAM PROCEDURE GETBITS(A,PW,DW);
BEGIN
LOCAL J,K;
SI←A; DI←PW; K←DI; DI←DW+J+DI;
SI←SI+10;
25(DI←K;
20(SKIP 47 DB; 1 BITS);
SKIP 35 SB;
5(SKIP 47 DB; 1 BITS);
K←DI; DI←J;
5(DI←DI+6; US←2 CHR);
J←DI; 2(SI←SI+50) );
END GETBITS;

```

```

BOOLEAN STREAM PROCEDURE LBL(A,B);
VALUE B;
BEGIN
SI←LOC B; SI←SI + 1;
DI←A;
IF 7 SC EQL DC THEN TALLY← 1;
LBL← TALLY;
END LBL;

```

```

PROCEDURE INPUT(RFC,ORBIT,SENSOR,E,X);
INTEGER REC,E,X;
ARRAY ORBIT,SENSOR(0,0);
BEGIN
REAL SUI;

```

```

LABEL MINN,WIS,MM;
LABEL HILD,UAHU,MAUI;
LABEL NT;
LABEL ARK;
LABEL VIX,PT;
LABEL OKLA;
LABEL WAX,NAN,NEW;
LABEL FJL,PARL;
LABEL EOF,PAR,LESS,HOME,FIVE,SIX,EIGHT,FOUR,SSP;
LABEL INT,TEN,THRTY;
ARRAY ALJ:375;
ARRAY J,EXLU:300;
ARRAY PWLO:6251,DWLO:1251;
ALPHA 35;
INTEGER W,C;
INTEGER M,J,P,K,I,L,N,F,W,FILES;
OWN REAL IST;
INTEGER TEST;
INTEGER S;
REAL D;
TEST← 0;
E←E+50;

```

ORIGINAL PAGE IS
OF POOR QUALITY

```

IF REC NEQ 0 THEN GO TO WIS ELSE
MINN: READ(1,375,AL*1) (EOF:PAR1)
E+0;
IF LBL(A,"ESSA ") THEN GO TO MINN ELSE GO TO THRTY;
VIX: S+1;
GO TO UNT;
WIS: S+0;
IF REC NEQ 1 THEN GO TO UNT ELSE
READ(1,375,AL*1) (EOF:PAR1);
UNT: READ(1,375,AL*1) (EOF:PAR1);
E+0;
IF S EQL 2 THEN GO TO TEN ELSE GO TO THRTY;
TEN: IF LBL(A,"ESSA ") THEN X+1 ELSE GO TO VIX;
IF TEST EQL 1 THEN X+2 ELSE GO TO EIGHT;
GO TO EIGHT;
THRTY: RESTRING(A,B,EX);
IF X EQL 1 THEN GO TO EIGHT ELSE
IF REC EQL 0 THEN GO TO PT ELSE
IF S EQL 1 THEN GO TO UNT ELSE
PT: FOR I=0 THRU THINGS-1 DO
BEGIN
BB← B(I);
J←(L+EX(I)*3"1766") DIV 3;
K←ABS(L) MOD 3;
IF K EQL 1 THEN BEGIN
BB.(10:38)←B.(19:38);
BB.(19:1)←0;
END ELSE IF K EQL 2 THEN
BEGIN
BB.(11:37)←BB.(19:37);
BB.(19:2)←0;
END;
BB .(12:7)←J.(14:16)+J.(11:7);
B(I)←BB;
END;
IF S/C EQL 0 THEN (27)←07.0 ELSE GO TO LESS;
TST← 101;
WRITE(1,"**KEY",FOR I=0 THRU 27 DO B(I),FOR J=0 THRU 321 DO 0 );
WRITE(LINE,"M14",FOR I=0 THRU 27 DO B(I));
GO TO EIGHT;
LESS:
BEGIN
GETBITS(A,PW,DW);
FOR J=0 THRU 24 DO
BEGIN
SUM←0.0;
N← J TIMES 12 + 9;
IF B(N) EQL 0.0 THEN X+1 ELSE GO TO OAHU;
N←J-1;
GO TO HILU;
OAHU: FOR I=0 THRU 4 DO
BEGIN
N← J TIMES 12 + I + 3;
ORBIT(I,1)←B(N);
END;
FOR N=J TIMES 25 + 20 THRU L+4 DO
SUM← SUM + PNLQ);
IF SUM EQL 0.0 THEN GO TO FIVE ELSE
FOR I=0 THRU 4 DO
SENSOR(I,1)←9999.0;
GO TO FOUR;
FIVE: FOR M=0 THRU 4 DO
BEGIN

```

ORIGINAL PAGE IS
OF POOR QUALITY

```

P← 5 TIMES J + M;
SENSOR(J,M)←0*(F);
IF SENSOR(J,M) LEQ 1024.0 THEN GO TO SIX ELSE
SENSOR(J,M)← SENSOR(J,M)-1024.0;
SIX: END;
FOUR: END;
END;
C← 4;
GO TO MAUI;
HILO: C← (N-4) DIV 5;
MAUI: FOR L←0 THRU C-1 DO
BEGIN
P← 5 TIMES L;
FOR I←2 THRU 4 DO
BEGIN
IF SENSOR(LP+I,0) NEQ 9999.0 THEN GO TO SSP ELSE
FOR M←0 THRU 4 DO
BEGIN
K← P + M;
FOR N←0 THRU 4 DO SENSOR(K,N)← 9999.0;
END;
SSP: END;
END;
IF REC LEN 2 THEN GO TO MM ELSE
IF REC GTR 9 THEN GO TO MM ELSE
FOR J←0 THRU 24 DO BEGIN
D← ORBIT(J,4);
IF D LSS 119.0 THEN GO TO WAX ELSE GO TO NEW;
WAX: IF SENSOR(J,1) LSS 350.0 THEN S←1 ELSE GO TO OKLA;
WRITE(LINE,</"..."TIME OUT OF SYNC...">/>);
WRITE(LINE,FMT10,REC);
X←2;
GO TO DNT;
NEW: IF D GTR 132.0 THEN GO TO WAN ELSE GO TO OKLA;
WAN: IF SENSOR(J,1) LSS 350.0 THEN GO TO OKLA ELSE
IF SENSOR(J,1) NEQ 9999.0 THEN S←1 ELSE GO TO OKLA;
WRITE(LINE,</"..."TIME OUT OF SYNC...">/>);
WRITE(LINE,FMT10,REC);
X←2;
GO TO DNT;
OKLA: END;
MM: IF X NEQ 1 THEN GO TO EIGHT ELSE
FOR I←N+1 THRU 24 DO BEGIN
FOR J←0 THRU 5 DO SENSOR(I,J)←0.0;
FOR K←0 THRU 6 DO ORBIT(I,K)←0.0;
END;
GO TO EIGHT;
EOF:
CLOSE(T,*);
WRITE(LINE,</"..."EOF...">/>);
E← E + 1;
IF E LSS 2 THEN GO TO MINN ELSE
IF 1ST LSS 3200.0 THEN GO TO MINN ELSE
GO TO EIGHT;

```

ORIGINAL PAGE IS
OF POOR QUALITY

```

EJFL:
CLOSE(T,*);

```

```

IF TEST EQL 1 THEN GO TO QT ELSE
IF REC LEQ 3 THEN TEST+1 ELSE GO TO ARK;
CLOSE(OT,*);
GO TO VIX;
ARK: IF X EQL 2 THEN CLOSE(OT,*) ELSE GO TO QT;
WRITE(LINE,</"...FOT..."/>);

GO TO EIGHT;
J1: WRITE(LINE,</"...EOT..."/>);

S+1;
E+ E + 1;
IF E LSS 2 THEN GO TO DNT ELSE
IF 1ST LSS 3200.0 THEN GO TO DNT ELSE X+3;
GO TO EIGHT;

```

```

PAR:
WRITE(LINE,</"...PAR..."/>);

E+0;
GO TO MINN;

```

```

PAR1:
WRITE(LINE,</"...PAR..."/>);

S+2;
E+0;
GO TO DNT;

```

```

EIGHT: END;

```

```

BEGIN
LABEL SIXTH;

LABEL ORE,OTE;
LABEL TEX,NM,AKIZ,COLD;
LABEL PARTA,PARTB,FIRST,SECOND,THIRD,SF;
LABEL BGM,BUFF,SCH,ALB,NY,ALO;
LABEL PBY,AYS;
LABEL IOWA,USN;
LABEL SAC,CAL,ARN,ARI,WACO,SASK;
LABEL SL;
LABEL ENG,SCOT;
INTEGER ARRAY CT(S1:150);
ARRAY TEMPL:150,1:7],TR(0:7,0:1000],T1R(0:7,0:500);
DEFINE T(T1,12)= TR(T2,T11#T1(T11,T12)= T1R(T12,T111)#;
INTEGER AB;
INTEGER Y,Z,CTS;
INTEGER I,J,K,L,M,P;
FOR J=1 THRU 150 DO BEGIN
READ(FILE5,FOT1, CT(S1)); FOR J=1 THRU 7 DO TEMPL(J);
IF I EQL 1 THEN GO TO SL ELSE
AB= CT(S1-J) + 10;
IF CT(S1) NEQ AB THEN GO TO ORE ELSE

```

ORIGINAL PAGE IS
OF POOR QUALITY

```

HL: END;
FOR I<=1 THRU 10 DO
BEGIN
FOR L<=1 THRU 10 DO
BEGIN
M<= 10 * I + (L-1);
U<=L;
V<= .1 * (U-1.0);
FOR J<=1 THRU 7 DO
BEGIN
IF TEMPI+J EQ 0.0 THEN GO TO ENG ELSE
IF M GTR 1000 THEN GO TO SCOT ELSE
IF TEMPI+1,J EQ 0.0 THEN GO TO ENG ELSE
TIK,J<= TEMPI,J + M * (TEMPI+1,J-TEMPI,J);
GO TO ENG;
SCOT: K<= M-1000;
IF TEMPI+1,J EQ 0.0 THEN GO TO ENG ELSE
TIK,J<= TEMPI,J + V * (TEMPI+1,J-TEMPI,J);
ENG: END;
END;
END;
FOR I<=1 THRU 7 DO BEGIN
LOCK(TP(I,*));
LOCK(TIK(I,*));
END;
CLOSE(FILE);
M<= 9999.0 TIMES .994;
SIXTH: REC<=1;
THIRD: M<=0;
FIRST: REC<=REC + 1;
INPUT(REC,ADMIT,SENSOR,E,X);
IF X EQ 2 THEN GO TO SIXTH ELSE
IF E EQ 2 THEN GO TO ONE ELSE
IF REC EQ 0 THEN GO TO FIRST ELSE
SECOND: REC<=REC + 1;
INPUT(REC,ADMIT,SENSOR,E,X);
IF X EQ 2 THEN GO TO SIXTH ELSE
IF E EQ 2 THEN GO TO ONE ELSE
PART:
FOR J<=0 THRU 23 DO
BEGIN
LABEL CHSTR,SCR,PITT,PHILA,PURT;
IF ASENSOR(J,1) EQ 0.0 THEN GO TO IDWA ELSE
IF ASENSOR(J,2) EQ 9999.0 THEN GO TO PHILA ELSE
IF ADMIT(J,4) LSS 115.0 THEN GO TO PITT ELSE
IF ASENSOR(J+1,2) EQ 9999.0 THEN GO TO CHSTR ELSE
DELTA<= ASENSOR(J+1,2)-ASENSOR(J,2);
DELTA<= ADMIT(J+1,4)-ADMIT(J,4);
DELTA<= ABS(ASENSOR(J,2)-ASENSOR(J,1));
IF M EQ 1 THEN GO TO SCR ELSE
IF DELTA< GTR 100.0 THEN M<=1 ELSE GO TO NB;
ASENSOR(J,2)<= ASENSOR(J,2) + 1024.0;
GO TO PHILA;
NB: IF DELTA< LSS 100.0 THEN M<=1 ELSE GO TO PITT;
GO TO PHILA;
CHSTR: FOR K<=0 THRU 4 DO ASENSOR(J,K)<= 9999.0;
GO TO PHILA;
SCR: IF SIGN(DELTA) GTR -1 THEN GO TO PHILA ELSE
IF DELTA< LSS -100.0 THEN M<=0 ELSE GO TO PURT;
GO TO PHILA;
PURT: IF ASENSOR(J,1) GTR 350.0 THEN M<=0 ELSE GO TO PHILA;
GO TO PHILA;

```

ORIGINAL PAGE IS
OF POOR QUALITY

PLT: ASENSOR(24,21) ASENSOR(24,21) + 1024.0;

PHLA: ASENSOR(24,21) 0;

END;

IF ASENSOR(24,21) EQL 9999.0 THEN GO TO NY ELSE

IF ASENSOR(24,21) LSS 115.0 THEN GO TO ALB ELSE

IF ASENSOR(24,21) EQL 9999.0 THEN GO TO RUFF ELSE

DELTA ← ASENSOR(24,21) - ASENSOR(24,21);

DELTA ← ABS(DELTA);

DELTA ← ABS(DELTA) - ASENSOR(24,21) - ASENSOR(24,21);

IF DELTA LSS 100.0 THEN M ← 1 ELSE GO TO BGM;

IF DELTA LSS 100.0 THEN M ← 1 ELSE GO TO BGM;

ASENSOR(24,21) ← ASENSOR(24,21) + 1024.0;

GO TO NY;

BGM: IF DELTA LSS 100.0 THEN M ← 1 ELSE GO TO ALB;

GO TO NY;

RUFF: FOR K ← 0 THRU 4 DO ASENSOR(24,K) ← 9999.0;

GO TO NY;

SCH: IF SIGN(DELTA) GTR -1 THEN GO TO NY ELSE

IF DELTA LSS -100.0 THEN M ← 0 ELSE GO TO ALO;

GO TO NY;

ALO: IF ASENSOR(24,11) GTR 350.0 THEN M ← 0 ELSE GO TO NY;

GO TO NY;

ALB: ASENSOR(24,21) ← ASENSOR(24,21) + 1024.0;

NY: ASENSOR(24,5) ← 0;

QRA: FOR K ← 0 THRU 4 DO

BEGIN

LABEL BRX,ELM;

P ← 5 × K;

IF ASENSOR(P+1,01) EQL 0.0 THEN GO TO PBY ELSE

FOR I ← 2 THRU 4 DO

BEGIN

IF ASENSOR(P+1,01) EQL 9999.0 THEN GO TO ELM ELSE

IF ASENSOR(P+1,01) LSS 400.0 THEN GO TO BRX ELSE

GO TO ELM;

BRX: ASENSOR(P+1,01) ← ASENSOR(P+1,01) + 1024.0;

ELM: END;

END;

PBY: FOR I ← 0 THRU 20 DO

BEGIN

LABEL SEM,HRT,ILL,AC;

FOR J ← 1 THRU 4 DO

BEGIN

CIS ← ASENSOR(I,J) TIMES .994;

IF CIS EQL 0 THEN GO TO TEX ELSE

IF CIS EQL 0 THEN GO TO TEX ELSE

IF CIS GTR 1000.0 THEN GO TO SLI ELSE

ASENSOR(I,J) ← CIS;

GO TO HRT;

SLI: CIS ← ASENSOR(I,J) - 1000.0;

IF CIS GTR 500 THEN CIS ← 500 ELSE GO TO AC;

AC: ASENSOR(I,J) ← CIS;

HRT: END;

ILL: END;

TEX: FOR K ← 0 THRU 4 DO

BEGIN

LABEL LA,NA,WD;

P ← 5 × K;

ORIGINAL PAGE IS
OF POOR QUALITY.


```

FOR I=2 THRU 4 DO
BEGIN
CTS← ASENSOR(I+1,0) TIMES .994;
IF CTS EQL 0 THEN GO TO NH ELSE
IF CTS EQL 1 THEN GO TO NH ELSE
IF CTS GTR 1000.0 THEN GO TO LA ELSE
ASENSOR(I+1,0)← T(CTS,I+3);
GO TO NH;
LA: CTS← ASENSOR(I+1,0)-1000.0;
IF CTS GTR 500 THEN CTS←500 ELSE GO TO WD;
WD: ASENSOR(I+1,0)← T(CTS,I+3);
NH: END;
END;

NM: WRITE(OT,*,*KEY, FOR I=0 THRU 24 DO LFOR J=0 THRU 5 DO AORBIT(I,J)
FOR K=0 THRU 5 DO ASENSOR(I,K));
IF X NEQ 1 THEN GO TO STE ELSE
CLOSE(OT,*)
GO TO SIXTH;
STE: REC← REC + 1;
INPUT(REC,AORBIT,ASENSOR,E,X);
IF X EQL 2 THEN GO TO SIXTH ELSE
IF E EQL 2 THEN GO TO URE ELSE
PARTBT
FOR J=0 THRU 23 DO
BEGIN
LABEL BC,SA,DALS,AUST,HSTN,SD;
IF BSENSOR(J,1) EQL 0.0 THEN GO TO USW ELSE
IF BSENSOR(J,2) EQL 9999.0 THEN GO TO SD ELSE
IF BORBIT(J,4) LSS 115.0 THEN GO TO HSTN ELSE
IF BSENSOR(J+1,2) EQL 9999.0 THEN GO TO DALS ELSE
DELTA← BSENSOR(J+1,2) - BSENSOR(J,2);
DELANG← BORBIT(J+1,4) - BORBIT(J,4);
DELTA← ABS(BSENSOR(J,2) - BSENSOR(J,1));
IF N EQL 1 THEN GO TO AUST ELSE
IF DELTA GTR 100.0 THEN N←1 ELSE GO TO SA;
BSENSOR(J,2)← BSENSOR(J,2) + 1024.0;
GO TO SD;
SA: IF DELTA LSS 100.0 THEN N←1 ELSE GO TO HSTN;
GO TO SD;
DALS: FOR K=0 THRU 4 DO BSENSOR(J,K)← 9999.0;
GO TO SD;
AUST: IF SIGN(DELANG) GTR *1 THEN GO TO SD ELSE
IF DELTA LSS *100.0 THEN N←0 ELSE GO TO BC;
GO TO SD;
BC: IF BSENSOR(J,1) GTR 350.0 THEN N←0 ELSE GO TO SD;
GO TO SD;
HSTN: BSENSOR(J,2)← BSENSOR(J,2) + 1024.0;
SD: BSENSOR(J,5)←N;
END;

IF BSENSOR(24,2) EQL 9999.0 THEN GO TO SAC ELSE
IF BORBIT(24,4) LSS 115.0 THEN GO TO CAL ELSE
IF ASENSOR(0,2) EQL 9999.0 THEN GO TO AMN ELSE
DELTA← ASENSOR(0,2) - BSENSOR(24,2);
DELANG← AORBIT(0,4) - BORBIT(24,4);
DELTA← ABS(BSENSOR(24,2) - BSENSOR(24,1));
IF N EQL 1 THEN GO TO WACU ELSE
IF DELTA GTR 100.0 THEN N←1 ELSE GO TO ABI;
BSENSOR(24,2)← BSENSOR(24,2) + 1024.0;
GO TO SAC;
ABI: IF DELTA LSS 100.0 THEN N←1 ELSE GO TO CAL;

```

ORIGINAL PAGE IS
OF POOR QUALITY

```

GO TO SAC;
ARR: FOR K=0 THRU 4 DO BSENSOR(24,K)+ 9999.0;
GO TO SAC;
WACO: IF SIGN(DELTA) GTR -1 THEN GO TO SAC ELSE
IF DELTA LSS -100.0 THEN M=0 ELSE GO TO SASK;
GO TO SAC;
SASK: IF BSENSOR(24,1) GTR 350.0 THEN M=0 ELSE GO TO SAC;
GO TO SAC;
CAL: BSENSOR(24,2)+ BSENSOR(24,2) + 1024.0;
SAC: BSENSOR(24,5)+M;
USK: FOR L=0 THRU 4 DO
BEGIN
LABEL SS,DENV;
P= 5 * L;
IF BSENSOR(P+1,0) FOL 0.0 THEN GO TO AYS ELSE
FOR I=2 THRU 4 DO
BEGIN
IF BSENSOR(P+1,0) FOL 9999.0 THEN GO TO DENV ELSE
IF BSENSOR(P+1,0) LSS 400.0 THEN GO TO SS ELSE
GO TO DENV;
SS: BSENSOR(P+1,0)+ BSENSOR(P+1,0) + 1024.0;
DENV: END;
END;

```

```

AYS: FOR I=0 THRU 24 DO
BEGIN
LABEL VA,WASH,IND,BR;
FOR J=1 THRU 4 DO
BEGIN
CTS= BSENSOR(I,J) TIMES .994;
IF CTS LQL 0 THEN GO TO ARIZ ELSE
IF CTS EQL H THEN GO TO IND ELSE
IF CTS GTR 1000.0 THEN GO TO VA ELSE
BSENSOR(I,J)+ T1(CTS,J);
GO TO WASH;
VA: CTS+ BSENSOR(I,J) - 1000.0;
IF CTS GTR 500 THEN CTS+500 ELSE GO TO BR;
BR: BSENSOR(I,J)+ T1(CTS,J);
WASH: END;
IND: END;

```

```

ARIZ: FOR K=0 THRU 4 DO
BEGIN
LABEL ORL,FLA,TTN;
P= 5 * K;
FOR I=2 THRU 4 DO
BEGIN
CTS= BSENSOR(P+1,0) TIMES .994;
IF CTS FOL 0 THEN GO TO COLD ELSE
IF CTS EQL H THEN GO TO FLA ELSE
IF CTS GTR 1000.0 THEN GO TO ORL ELSE
BSENSOR(P+1,0)+ T1(CTS,I+3);
GO TO FLA;
ORL: CTS+ BSENSOR(P+1,0)-1000.0;
IF CTS GTR 500 THEN CTS+500 ELSE GO TO TTN;
TTN: BSENSOR(P+1,0)+ T1(CTS,I+3);
FLA: END;
END;

```

ORIGINAL PAGE IS
OF POOR QUALITY

```

COLD: WRITE(OT,**KEY, FOR I=0 THRU 24 DO [FOR J=0 THRU 6 DO BORBITLI,J],

```

```
FOR K=0 THRU 5 DO HSENSOR(I,K));  
IF X NEQ 1 THEN GO TO SECOND ELSE  
CLOSE(OT,*);
```

```
SF:  
GO TO SIXTH;
```

```
DRE:  
CLOSE(OT,*);  
IF X EQL 3 THEN CLOSE(OT,*) ELSE  
END;
```

```
END.
```

ERRORS DETECTED = 0. COMPTLATION TIME = 25 SECONDS.

109; TOTAL SEGMENT SIZE = 1171 WORDS; DISK SIZE = 61 SEGS; NU. PGM. SEGS = 31

DRE STORAGE REQUIRED = 6882 WORDS.

AUXILIARY MEMORY REQUIRED = 0 WORDS.

ARD-IMAGES PROCESSED = 520.

00000/LINE 731387USER=PH3144;COMPILE UCHAREQ/PH3144 XALGOL .KOHFI, BILL

00000/LINE 731387USER=PH3144;COMPILE UCHAREQ/PH3144 XALGOL .KOHFI, BILL

ORIGINAL PAGE IS
OF POOR QUALITY